Die approbierte Originalversion dieser Diplom-/ Masterarbeit ist in der Hauptbibliothek der Technischen Universität Wien aufgestellt und zugänglich.
http://www.ub.tuwien.ac.at

The approved original version of this diploma or master thesis is available at the main library of the Vienna University of Technology.
http://www.ub.tuwien.ac.at/eng

TECHNISCHE UNIVERSITÄT WIEN
Vienna University of Technology

DIPLOMARBEIT

Location of solar potential on rooftops by application of different methodologies

Ausgeführt am Institut für

Geodäsie und Geoinformation

Der Technischen Universität Wien

Unter der Anleitung von **Ao.Univ.Prof.i.R. Dipl.-Ing. Dr.techn. Josef Jansa** und **Dr.techn. Dipl.-Ing. Camillo Ressl**

durch

Markus Konopiski

Hauptplatz 3, 2870 Aspang

Datum: 20. 10. 2015 **Unterschrift**

Abstract

In this thesis three different methodologies to assess solar irradiation values of rooftops for specific days throughout a test area are implemented, and the resulting outputs are compared with each other. The irradiation values are visualized in a raster map. A high number of different approaches in the estimation of solar irradiation in large scale applications is available for several software programs. The test area in this thesis is located in the 9th district of Vienna, has primarily residential character and a rather sparse distribution of vegetation. Trees are assumed to be an important factor in influencing the solar irradiation performance on roofs in general. The basis of the computations constitutes a dense three-dimensional point cloud which was recorded by an airborne laser scanner. The point cloud has to be transformed into an elevation model to enable further processing steps in all three software programs. Besides ArcMap and QGIS that offer highly accurate tools for various applications of solar radiation calculations, a new program that is still in its development phase, namely VOSTOK, is included in this thesis.

Vegetation has a significant influence on the annual solar irradiation in the observed test area. Therefore a Digital Surface Model (DSM), that includes vegetation, serves as the basic elevation model. Since VOSTOK is not able to compute solar irradiation values for the whole test area, a subset area is selected to enable a meaningful comparison. This area yield solar irradiation values for all pixels in every program. Unlike VOSTOK, ArcMap and QGIS provide editable parameters which describe the state of the atmosphere and the reflection properties of the Earth surface. The programs use different algorithms to yield solar irradiation. In the first calculation step the calculation is performed with the default values for ArcMap and QGIS. The results for QGIS and VOSTOK show a high similarity. After that the atmospheric influence and the ground reflection are excluded from the computations. The irradiation maps have a high correlation for the analysed days. The assumption is made that the similarity between default parameters and the implemented algorithm in QGIS and VOSTOK is high, due to their similar results. All resulting maps are analysed by means of statistical calculations to yield their degrees of correlation.

Kurzfassung

Im Zuge dieser Diplomarbeit werden drei verschiedene Methoden zur Abschätzung der Solaren Einstrahlungswerte auf Dachflächen für bestimmte Tage in einem Testgebiet implementiert und deren Resultate miteinander verglichen. Die Einstrahlungswerte werden in einer Rasterkarte visualisiert. Für die Abschätzung der Solaren Einstrahlung im großen Maßstab gibt es bereits eine Reihe verschiedener Herangehensweisen, die mit unterschiedlichen Programmen realisiert werden können. Die Testregion für diese Arbeit liegt im neunten Bezirk der Stadt Wien und besteht mehrheitlich aus Wohnhäusern und vereinzelten Vegetationsflächen. Bäume werden generell als signifikanter Einflussfaktor für die solare Einstrahlungsleistung auf Dächern angenommen. Die Grundlage der Berechnungen stellt eine drei-dimensionale Punktwolke dar, die mittels airborne laser scanning aufgenommen wurde. Diese Punktwolke muss in ein Höhenmodell umgewandelt werden, um weitere Prozessierungsschritte in allen drei Programmen zu ermöglichen. Neben ArcMap und QGIS, welche äußerst genaue Tools für verschiedene Anwendungen anbieten, wird ein neues Programm, namens VOSTOK, das noch in der Entwicklungsphase ist, in der Diplomarbeit mit einbezogen.

Vegetation hat in dem beobachteten Testgebiet einen signifikanten Einfluss auf die jährlichen Sonneneinstrahlungswerte. Deshalb dient ein Digitales Oberflächen Modell (DOM, englisch: Digital Surface Model - DSM) als grundlegendes Höhenmodell. Da VOSOTK nicht in der Lage war Einstrahlungswerte für die gesamte Testregion zu berechnen, wurde ein Ausschnitt der ursprünglichen Fläche gewählt, um einen sinnvollen Vergleich zwischen den Programmen zu ermöglichen. Diese Fläche liefert Solare Einstrahlungswerte für jeden Pixel in allen Programmen. ArcMap und QGIS bieten die Möglichkeit Parameter, die den Zustand der Atmosphäre und die Reflexionseigenschften der Erdoberfläche beschreiben, zu editieren. Die Programme verwenden unterschiedliche Algorithmen zur Berechnung der Einstrahlung. Im ersten Berechnungsschritt wurden die Default-Werte in ArcMap und QGIS für die veränderbaren Parameter verwendet. Die Ergebnisse von QGIS und VOSTOK weisen eine hohe Ähnlichkeit auf. Danach werden der atmosphärische Einfluss und die Bodenreflexionen durch Anpassung der entsprechenden Parameter von der Berechnung ausgeschlossen. Nun korrelieren die Einstrahlungskarten von ArcMap und QGIS stark. Es kann angenommen werden, dass durch die große Ähnlichkeit der Resultate für einzelne Tage in QGIS und VOSTOK, die Default-Werte und die implementierten Algorithmen vergleichbar sind. Alle

durch die Berechnungen entstandenen Rasterkarten wurden mittels statistischer Berechnungen auf ihre Korrelation geprüft.

Acknowledgements

Initially, I would like to thank my girlfriend Dimitra, my mother Christine and my grandmother Marianne for all their support and patience throughout this entire process.

I would also like to thank Professor Josef Jansa for guiding and supervising me through my thesis. He helped me to solve problems and was always able to give me a positive feeling about my work.

Furthermore I would like to thank Dr. Bernhard Höfle and Sebastian Bechtold from the Heidelberg University for providing necessary information and data to include the prototype program VOSTOK in the practical part of my thesis.

Table of Contents

1. INTRODUCTION 1
1.1. Motivation 1
1.2. Goal of Work 1
1.3. Hypothesis 2
1.4. Renewable Energy 2
1.4.1. Solar Energy 3
1.4.2. Wind Energy 4
1.4.3. Other types of Renewable Energy 4
1.4.4. Renewable Energy in Austria 5
1.5. Solar Energy in urban areas 6
1.6. Solar Radiation Basics 7
2. LITERATURE REVIEW 9
2.1. PV Potential on Rooftops – Applied Methods 9
2.1.1. Constant-Value Methods 9
2.1.2. Manual Selection Methods 10
2.1.3. GIS Based Methods 11
2.2. Solar Energy Collectors 13
2.3. Solar Radiation Models 14
2.4. Components of Solar Radiation 16
2.4.1. Beam radiation 16
2.4.2. Diffuse radiation 18
2.4.3. Ground reflected radiation 18
2.5. Solar Radiation Online Tools 20
2.5.1. PVWatts simulation tool 20
2.5.2. PV-GIS 21
3. MAJOR CHALLENGES 23
3.1. Solar Radiation Recording 23

3.1.1. Solar Radiation derived from airborne LIDAR measurements 24
3.1.2. Ground Measurements of Solar Radiation 24
3.1.3. Solar Radiation derived from Satellite Observations 25
3.2. Delineation of Rooftops 26
3.2.1. Generation of 3D Elevation Models 26
3.2.2. Classification of Urban Areas 28
4. METHODS 31
4.1. Test Area and Data 31
4.2. Generation of a Roof-filtered Irradiation Map 32
4.3. Calculation of the Solar Potential Map 34
4.3.1. Arcmap's Solar Potential Map 36
4.3.2. QGIS's Solar Potential Map 40
4.3.3. VOSTOK's Solar Potential Map 43
4.4. Comparison of the methods 45
5. RESULTS AND INTERPRETATION 47
5.1. The Influence of Vegetation 48
5.2. Comparison of the Equinoxes 51
5.3. Solar irradiation comparison 52
5.4. Deactivation of the atmospheric influence 57
6. DISCUSSION 60
7. CONCLUSION 62

List of Tables

Table 1: Share of renewable energy in gross inland consumption, 2012 in % (Eurostat 2015) 5
Table 2: Advantages and disadvantages of rooftop area estimation methods (Melius et al. 2013) 12
Table 3: Important input parameters for ArcMap Solar Analysis 39
Table 4: Outputs of the area solar radiation analysis in ArcMap 39
Table 5: Mandatory inputs for r.sun (Hofierka and Suri 2002) 41
Table 6: r.sun outputs for mode 1 (Hofierka and Suri 2002) 42
Table 7: r.sun outputs for mode 2 (Hofierka and Suri 2002) 42
Table 8: Important input parameters for VOSTOK 44
Table 9: Editable atmospheric and surface parameters 46
Table 10: Statistical measures of the solar irradiation map, calculated with VOSTOK (21st of March) 47
Table 11: Results of statistical calculations of the annual (2015) irradiation maps 48
Table 12: Statistical Parameters of 4 different solar irradiation maps on March 21st – Arcmap with atmosphere and surface reflection, Arcmap without atmosphere and surface reflection; the sam for QGIS 58

List of Figures

Figure 1: Extraterrestrial solar spectrum and terrestrial standard solar spectrum (Paulescu et al. 2013) 8
Figure 2: Components of solar radiation on the earth's surface (Vardimon 2011) 16
Figure 3: The averaged annual sum (4.2004 – 3.2010) of Austria's Global horizontal radiation (http://solargis.info/doc/free-solar-radiation-maps-GHI) 17
Figure 4: relevant angles for solar radiation **(Paulescu 2013)** 19
Figure 5: PVWatts results for a PV system of approximately 25 m² in New York City **(http://pvwatts.nrel.gov/)** 21
Figure 6: Distribution of the WRDC network (Paulescu 2013) 25
Figure 7: Basic idea of a morphological filter 27
Figure 8: a) Assessment of echo ratio value for single laser points of a point cloud; b) slope adaption depending on local surface slope **(Höfle et al. 2009)** 29
Figure 9: Test area in the 9th district of Vienna 31
Figure 10: Histogram of the distribution of the point density (laser points per m²) 32
Figure 11: Echo ratio map of the test area 33
Figure 12: Flowchart, describing the generation of a roof map 34
Figure 13: Analysis of the vegetation's influence 35
Figure 14: Assessment of a solar irradiation map for roof areas only 36
Figure 15: Calculation of a hemispherical viewshed for one point of a DEM 37
Figure 16: ArcMap Processing Model 40
Figure 17: QGIS Model to obtain a solar irradiation map 43
Figure 18: Vostok Model to estimate a solar irradiation map 44
Figure 19: Solar irradiation map without any influence of objects outside the rooftop area 49
Figure 20: Solar irradiation map with the influence of objects outside of the rooftop area 49
Figure 21: Solar irradiation difference map. Vegetation excluded minus vegetation included 50
Figure 22: Comparison of the solar irradiation performance of the spring and autumn equinox of the year 2015 51
Figure 23: Distribution of sola irradiation values for both equinoxes 52
Figure 24: Histogram of global irradiation values for the 21st of March obtained with ArcMap's solar analysis tool, QGIS r.sun and Vostok 54
Figure 25: Relative comparison of QGIS and ArcMap solar irradiation map for the 21st of March through a cross-correlation. A sample of 50,000 pixels was selected randomly. 56

Figure 26: Relative comparison of QGIS and ArcMap solar irradiation map for the 21st of June through a cross-correlation. A sample of 50,000 pixels was selected randomly. 56
Figure 27: Relative comparison of QGIS and ArcMap solar irradiation map for the 21st of December through a cross-correlation. A sample of 50,000 pixels was selected randomly. ... 57
Figure 28: Histograms of the solar irradiation maps without atmospheric effects on the irradiation performance 59

1. INTRODUCTION

1.1. Motivation

Anthropogenic climate change and the harmful consequences for the environment due to the global increase of greenhouse gases in the atmosphere has been discussed over many years. Even though a lot of scientists proved the human responsibility by means of different researches, the countries efforts to reduce CO_2 concentrations remain rather low. Therefore it is of significant importance to call as much attention as possible to strategies that aim to reduce greenhouse gases. Renewable energy not only decreases these gases but is also free of limitations as long as our planet exists.

In particular solar energy has a big potential in urban areas, where solar radiation exploitation systems can be installed on rooftops or facades. "Solar cities" is an emerging concept which attempts to demonstrate that passive and active solar techniques are able to contribute significantly to the energy balance of urban areas (Hofierka and Kanuk 2009). Suri et al. (2007) states that the average area of photovoltaic (PV) modules mounted at the optimum angle in the member states of the European Union and candidate countries would not exceed 0.6% of the total territory on average.

1.2. Goal of Work

The goal of this research is to evaluate and compare solar irradiation maps for rooftops in an urban test area in the city of Vienna, which are obtained by different software programs. Solar irradiation maps for single days are assessed and output as values of irradiation in Wh/m²/day for each pixel in a raster map. The resulting maps include values for roof areas only and are expected to yield information about the exact methodology of the different programs. The basis of the research is a three-dimensional point cloud with a high resolution that has been recorded by an airborne laser scanner. In order to archive this goal a conceptual analysis model for the estimation of incoming solar irradiation and comparison of the results will be developed. To perform this estimation analysis, models integrated in a Geographic Information System (GIS) are implemented. The comparison is carried out by a statistical pixel-wise analysis of the results.

1.3. Hypothesis

The estimation of solar irradiation performed by different analysis models of distinct programs leads theoretically to the same, practically to similar irradiation values in the resulting raster maps.

1.4. Renewable Energy

All energy used on our earth originates from one of the following sources: Radiant energy emitted by the sun; geothermal energy from the interior of the earth; tidal energy originating from the gravitational forces of the moon; and nuclear energy. The largest source is solar energy, which is thousand times stronger than all the others. The present energy system that is essentially based on the use of fossil fuels is not able to address many problems very well. Non-renewable energy systems yield environmental damage and health issues. Anthropogenic greenhouse gases are changing the atmosphere in a way that is affecting the climate. Current CO_2 emission trends will lead to more than a doubling of atmospheric concentrations before 2050. The International Panel on Climate Change (IPCC) shows evidence and connections considering climate change in its publications. In their fifth assessment report (IPCC 2014) the following statements are presented:

- In recent years climate change have caused impacts on natural and human systems on all continents and across the oceans.
- In many regions a change of precipitation altering the hydrological systems was observed.
- Many species have changed their behaviour in response to ongoing climate change.
- Crop yields have experienced more negative than positive changes.

Renewable energy is created by sources which are naturally replenished. On the contrary, fossil fuels are non-renewable and will either be too expensive or impossible to extract in the future. There is no strict definition of the term renewable energy but the most types come from weather phenomena, like heat of the sun, wind or rainfall. Currently the use of renewable energy accounts only for a few percent compared to fossil systems.

1.4.1. Solar Energy

Solar Energy can be used for heating houses or water, and for generating electricity. This form of energy belongs to renewable resources because it is continuously supplied to the earth by the sun (Spellman and Bieber 2011). Solar Energy uses different technologies to take advantage of the sun's radiation, used either for space and water heating or to produce electricity. The two most important solar energy technologies to generate electricity are concentrating solar power (CSP) and photovoltaics (PV).

Concentrating solar power (CSP) systems produce power by using mirrors to concentrate sunlight onto a thermal receiver. The receiver absorbs the radiation and converts it into heat. With the higher temperature it is possible to start a turbine or an engine that produces electricity. Typically CSP plants are equipped with sun tracking devices to follow the sun, both seasonally and throughout the day, to improve the system's electrical output. Photovoltaic panels convert the ultraviolet part of sunlight directly into electricity at the atomic level. Some materials are able to perform the photovoltaic effect. This effect causes absorption of photons of light and releases electrons. The free electrons yield an electric current that can be used as electricity. Solar cells are made of semiconductor materials, like silicon, germanium, gallium arsenide, and silicon carbide. The utilization of solar photovoltaic energy is the fastest growing energy source on a global scale (Chen 2011, p 3).

The average power density of solar radiation on the outside border of the atmosphere is near to 1366.1 W/m² according to data collected over 25 years from terrestrial and space observations (Paulescu et al. 2013). This value is known as the solar constant. Not all solar radiation falling on the atmosphere reaches the earth's ground. About 30% is reflected into space and about 20% is absorbed by clouds and molecules in the air (Chen 2011, p 2). Freris and Infield (2008, p 36) claim that an area of 5 km² would be needed to produce a gigawatt of power (assuming a conversion efficiency of 20%). Especially in countries with high population densities and low irradiance values rooftop installations of solar energy systems are logical.

1.4.2. Wind Energy

The warming of the atmosphere by solar radiation leads to turbulences that cause winds. The Earth's atmosphere is constantly in motion, vertically and horizontally. There are two forces that appear in the atmosphere; gravitation and pressure differences caused by temperature variations. Wind energy is the process by which the movement of air is used to generate mechanical power or electricity. Temperature differences between equatorial regions and areas further north or south lead to global wind systems. Near the equator warm air rises to high altitudes and then flows northwards and southwards where the air near the surface is cooler. This movement ends at about 30°N and 30°S respectively. Air begins to cool and sink and a returned movement of the cooler air takes place close to the surface of the Earth. Therefore equatorial areas are low pressure zones. Regions where air is descending are high pressure areas. This pressure gradient forces the flow of the air from high to low pressure. Additionally to global wind systems that are caused by temperature gradients local varieties can be observed. The local topography influences air movement as well as objects like buildings and trees.

The high variability of wind speed and direction causes problems in prediction for a specific location. This can have a negative effect on the performance of electricity production. The time scales of this variability reaches from annual changes to changes in between seconds (turbulences). Wind energy is captured by systems called wind turbines. These systems are designed to generate their rated output at a rated wind speed. For wind speeds below a certain value the turbine is not operational. (Freris and Infield 2008)

1.4.3. Other types of Renewable Energy

Hydropower is indirectly linked to solar energy which evaporates the water in the oceans, which is then transported to land masses as rain and forms rivers. Hydroelectric plants (dams) are built on rivers to create reservoirs. These reservoirs guarantee constant water supply for electricity generation on demand.

Another type of renewable energy, namely **bioenergy**, burns biomass to generate power. Former living materials can be considered as biomass, which is mainly produced by photosynthesis from the sun's radiation. Biomass can also be converted into liquid biofuels that can be used for transport. **Geothermal energy** extracts the natural heat of the Earth to use it for heat or electricity production. Tidal forces and waves of the oceans are also considered

as sources of renewable energy. This type of renewable energy is called **ocean energy**. (Assmann et al. 2006)

1.4.4. Renewable Energy in Austria

In March 2007 all EU countries formally agreed on increasing the share of renewable energy to 20% until 2020 (Fink et al. 2008). The share of renewable energy in gross inland energy consumption in the year 2012 for Austria was 30.1% (table 1). The EU's average was 11.0%. Thus, compared to other countries of the EU, Austria's usage of renewable energy is above average, especially due to high values in biomass energy and hydropower which are the major types for renewable energy in Austria. 17.5% of the whole energy in 2012 was delivered by biomass and renewable waste and hydropower constitute 11.2%, according to Eurostat (Eurostat 2015). Solar Energy has a small contribution of 0.6% of total energy consumption. The EU's average share of solar energy is 0.5%. On the global market Israel and Cyprus have by far the highest values in solar energy per capita, and China in total numbers.

	Renewable energy total	Biomass & renewable wastes	Hydropower	Geothermal	Wind	Solar
EU-28	11.0	7.3	1.7	0.3	1.1	0.5
Euro area (EA-18)	11.1	7.1	1.6	0.5	1.2	0.7
Belgium	5.9	5.1	0.1	0.0	0.4	0.4
Bulgaria	8.9	6.2	1.5	0.2	0.6	0.5
Czech Republic	7.5	6.5	0.4	0.0	0.1	0.5
Denmark	23.3	18.2	0.0	0.0	4.9	0.2
Germany	10.4	7.5	0.6	0.0	1.4	0.9
Estonia	14.1	13.4	0.1	0.0	0.6	0.0
Ireland	5.9	2.9	0.5	0.0	2.5	0.1
Greece	9.6	5.6	1.4	0.1	1.2	1.2
Spain	12.6	5.9	1.4	0.0	3.3	1.9
France	8.2	5.5	2.0	0.1	0.5	0.2
Croatia	12.1	6.7	4.9	0.1	0.3	0.1
Italy	12.7	5.7	2.1	3.0	0.7	1.1
Cyprus	5.1	1.8	0.0	0.1	0.6	2.6
Latvia	36.4	29.2	7.0	0.0	0.2	0.0
Lithuania	16.4	15.2	0.5	0.1	0.7	0.0
Luxembourg	3.1	2.7	0.2	0.0	0.1	0.1
Hungary	7.5	6.7	0.1	0.5	0.3	0.0
Malta	1.1	0.8	0.0	0.0	0.0	0.2
Netherlands	4.3	3.7	0.0	0.0	0.5	0.1
Austria	30.1	17.5	11.2	0.1	0.6	0.6
Poland	8.8	8.2	0.2	0.0	0.4	0.0
Portugal	10.8	12.6	2.2	0.6	4.0	0.5
Romania	14.7	11.0	2.9	0.1	0.6	0.0
Slovenia	14.8	9.3	4.8	0.5	0.0	0.3
Slovakia	8.1	5.7	2.1	0.0	0.0	0.3
Finland	29.2	24.8	4.3	0.0	0.1	0.0
Sweden	37.2	22.3	13.6	0.0	1.2	0.0
United Kingdom	4.1	3.0	0.2	0.0	0.8	0.1

Source: Eurostat (online data codes: nrg_100a and nrg_107a)

Table 1: Share of renewable energy in gross inland consumption, 2012 in % (Eurostat 2015)

1.5. Solar Energy in urban areas

According to Hofierka and Kanuk (2009), more than 80% of inhabitants of the most developed countries live in urban environments. That leads to the fact that most of the energy is consumed at the same place where huge amounts of greenhouse gases are produced, namely in cities. In that sense it seems reasonable to locate energy generating systems in, or close to urban areas. Renewable energy systems, which exploit solar energy can be installed on rooftops or facades to reduce greenhouse gases and deliver "clean energy". These systems can either be photovoltaic modules (PV) or solar thermal energy panels (ST). PV converts sunlight into electricity using a semiconductor material. ST panels are made of specific material to maximize the absorption of sunlight and convert it into heat.

For researchers who investigate the potential of rooftop-installed photovoltaic panels (PV), it is crucial to understand the amount and characteristics of rooftop space that is available for installing PV. Many methods of estimating rooftop areas have been developed, ranging from simple multipliers to methods that use complex geographic information systems (GIS) or three-dimensional models (Chaves and Bahill 2010). A detailed discussion about different methods that were used in former studies can be found in chapter 2.

The basis of a GIS based calculation of solar energy potential in urban areas with high spatial and temporal resolution is a three dimensional model, that represents the earth surface, including the top surfaces of buildings and vegetation. This kind of model is called digital surface model (DSM) and is most commonly derived from a point cloud recorded by an airborne laser scanner. Laser scanning is an active remote sensing method that measures single points to delineate the geometry of the earth surface.

The most important parameter for the calculation of solar potential is the amount of solar irradiation that hits a roof area within a specific time unit. The problems of this parameter are the strong spatial and temporal variations that are caused by changing atmospheric, e.g. clouds, aerosols, water vapour, temperature, ozone, and local illumination conditions like shades caused by varying angles of incidence and shadows. Therefore the solar irradiation is dependent on atmospheric conditions, temporal variations, and different roof characteristics like:

- Elevation: The location should be on top of a building.
- Orientation: The orientation of the surface should be south facing for the northern hemisphere.
- Slope: The slope should not be too steep. The optimal roof inclination for the countries of the European Union lies between 33 and 42 degrees.
- Area: The area that receives enough solar irradiation should have a certain expansion.

In general the goal is to find rooftops that face south, have a slope that has an inclination close to the optimal value and a rather big expansion. The site should at least receive some minimum threshold of solar radiation each year (Melius et al. 2013).

1.6. Solar Radiation Basics

The sun fills the surrounding space continually with energetic elementary particles and photons of electromagnetic radiation. The sun's electromagnetic spectrum at the earth's surface is only a small subset of its total spectrum due to attenuation of the atmosphere. It is called optical solar radiation even though it ranges from the UV wavelengths to the near- and mid-infrared region. (Myers 2013) This is the area of the electromagnetic spectrum from 0.29μm until 4μm. The amount of solar energy at the surface of the earth beyond 2.5μm is very small.

The magnitude of solar radiation reaching the earth's surface depends on the location. Solar radiation is further affected by the earth's rotation and revolution around the sun as well as environmental factors such as atmospheric attenuation effects, caused by clouds and water vapour. (Fu and Rich. 1999) On the ground, topography influences the amount of solar radiation reaching a specific surface. These topographic parameters are the elevation, slope, and orientation of the site.

Irradiance: It is the flux of optical solar radiation, i.e. the energy, falling on unit area per unit time. The S.I. units for irradiance are joules per second per square meter or watts per second per square meter (W/m^2). Irradiance is the power of solar radiation on the earth's surface per unit area.

Irradiation: The amount of solar power falling on unit area over a stated time is called irradiation. Thus it is the integral of the irradiance with respect to time. Its unit is watt hours per square meter (Wh/m²). Irradiation is the energy of solar radiation reaching the earth's surface. (Page 1986)

Solar Constant: In a point at the top of the Earth's atmosphere, the beam of incident sunrays is referred to as Extraterrestrial Radiation (ETR). ETR fluctuates about 6.9% during the year due to the varying distance between the Earth and the Sun. Figure 1 depicts the spectral distribution of ETR at the mean Sun-Earth distance with and without atmospheric influences. AM1.5G represents the terrestrial standard solar spectrum defined by the Commision Internationale de l'Eclairage (CIE) and the American Society for Testing and Materials (ASTM). The integration of the extraterrestrial solar spectrum over all wavelengths defines the solar constant G_{SC}. Since the Sun's radiance varies, the solar constant also changes over time. Paulecu et al. (2013) mentions that the actual best estimate for the average solar constant is 1366.1 W/m². This value is based on data collected over 25 years from terrestrial and space observations.

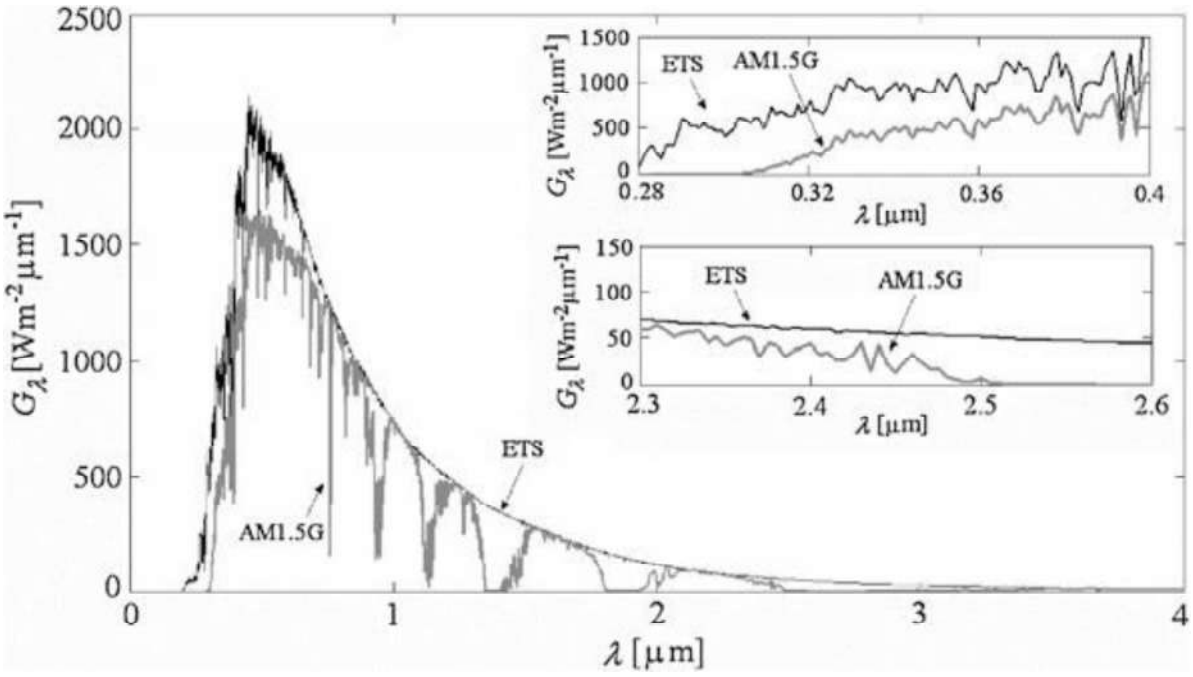

Figure 1: Extraterrestrial solar spectrum and terrestrial standard solar spectrum (Paulescu et al. 2013)

Ultraviolet and Infrared spectral domains are presented in the right upper corner in detail.

2. LITERATURE REVIEW

2.1. PV Potential on Rooftops – Applied Methods

According to a report from Melius et al. (2013), which serves as basis for this chapter, there are three major rooftop-area estimation methods to assess the available solar radiation. The report reviews 35 studies and 6 patents. Many methods have been developed, ranging from simple multipliers of total building space to methods that employ complex geographic information systems (GIS) or three-dimensional models. A classification of different methods is described in the following chapters. In addition, some examples of already applied studies are given.

2.1.1. Constant-Value Methods

The significant advantage of constant-value methods is their ease of use. They are neither time- nor resource-intensive and constitute a useful basis for solar potential calculations throughout a whole region. Many of these methods consider typical rooftop configurations and apply these estimations on a specific area. Furthermore these studies often use rules-of-thumb assumptions about roof characteristics. A variation of the constant-value method that could lead to more accurate results is an estimation based on the region's population density. An important drawback of constant-value methods are their generalized results which do not consider rooftop characteristics for individual buildings and are difficult to validate.

Examples:

In a report written by Navigant Consulting, Inc. (Navigant Consulting 2007) floor-space data of California is used to extrapolate total rooftop area from total floor area. In addition weather data from typical meteorological year (TMY2 or TMY3) are implemented to estimate solar resource. Rooftops are divided into residential and commercial roofs. The study concludes that 60% to 65% of commercial rooftop space and 22% to 27% of residential rooftop space is suitable for PV, depending on whether the climate is warm or cold.

In other studies more general estimating approaches are applied. Vardimon (2011) uses building data and shapefiles to calculate rooftop area in Israel. In this study rooftops are classified in commercial, residential and industrial roofs. A constant value of 30% of suitable roof areas is applied on all buildings. This yields to an energy potential production by means of PV-panels of 32% of Israel's total electricity consumption.

2.1.2. Manual Selection Methods

Manuel selection methods yield more detailed results than constant-value methods. Their main disadvantage is the distinct increase in time exposure. Many approaches use aerial imagery to manually select rooftop areas based on their solar resource which can be measured by meteorological stations. Another criterion for suitable roofs is their location characteristics, like orientation and angle. In addition, other parameters such as land use, objects that causes shadows, and the loss of PV-performance can be considered in the process of selecting suitable roof areas. The footprints of PV-suitable buildings are digitized and their rooftop area is calculated.

Many studies use online tools such as Google Earth to select suitable roofs. Similar to the aerial imagery approaches these studies derive the PV-suitability of rooftops by visually inspecting shadow causing objects and building obstructions.

Example:

Studies in Vienna (Wittmann and Bajons 1997) measure roofs of buildings in the eight district of Vienna with respect to their position, size, inclination and azimuth by means of photogrammetry. For simplification roof surfaces are divided into triangles. Basically the determination of local roof area by photogrammetry is an objective method nevertheless some subjective decisions have to be made. Average solar radiation data from the Austrian catalogue of climatic data was applied in the calculations.

2.1.3. GIS Based Methods

In contrast to the already described methods, GIS based approaches feed ideal rooftop characteristics into a computer model and a GIS software determines areas of high suitability. Therefore they are more objective, quicker, and lead to more accurate results. However, GIS based methods are time- and computer resource-intensive processes.

The basis of GIS based methods is usually a 3D-model, which can be used to evaluate solar resource or shadow effects in build-up areas. They are most likely generated from stereo aerial pictures through matching or point clouds recorded by LiDAR (light detection and ranging) techniques. In this thesis the GIS-based method based on a 3-D model derived from a LIDAR point cloud is applied and will be described in more detail in chapter 4.

Examples:

In a study by Hofierka and Kanuk (2009) in Bardejov, Slovakia a three dimensional model is created by collecting different kinds of data that yield information about the surface structure. The data included topographic maps, orthophotomaps and large-scale city maps. The solar resource of a test area is calculated based on this 3D-model that is generated by the programs GRASS GIS and ArcView GIS. This yields a solar radiation map of the city. In the end the solar radiation map is implemented in PVGIS, a program to estimate energy potential using GIS data. The study concludes that 45% of the total current energy consumption of Bardejov could be produced only by rooftop installed PVs.

Another study in Vancouver (Tooke et al. 2011) uses the ArcGIS solar analyst tool to find roof areas with high solar potential. LiDAR data is used to generate a 3D model. The laser was configured to record first, second and last return laser hits and ground and non-ground hits were classified using in-house software. The solar radiation is estimated by the Solar Analyst tool along with local weather data. The study concludes that trees reduce solar radiation on rooftops by an average of 38%.

The program RADIANCE/DAYSIM is used in an analysis in Fribourg, Switzerland (Compagnon 2004). The functionality of this program is the simulation of lighting scenarios. A 3-D model is run through RADIANCE/DAYSIM and a minimum of 1000 kilowatt-hours per square meter (kWh/m²) is defined as a threshold to determine suitable rooftop areas. The study concludes that the potential for PV systems on roofs lies between 6.5% and 21% of total roof area.

Estimation Methods	**Advantages**	**Disadvantages**
Constant-value method	Quick and easy to compute	Generalized results do not consider localized rooftop characteristics Results are difficult to validate
Manuel selection method	Detail-specific Enables assumptions based on specific knowledge of regions and buildings	Time intensive Not easy to replicate across multiple regions
GIS based method	Detail-specific Replicable across multiple regions Possibility for automation	Time intensive Computer-resource intensive

Table 2: Advantages and disadvantages of rooftop area estimation methods (Melius et. al 2013)

2.2. Solar Energy Collectors

Solar Energy Collectors are instruments that transform solar radiation energy to internal energy. The major component of any solar system is the solar collector. This device absorbs the incoming solar radiation, converts it into heat, and transfers the heat to a fluid flowing through the collector for storage or instant use.

There are basically two types of solar collectors: non-concentrating or stationary, and sun-tracking concentrating. A non-concentrating collector has the same area for intercepting and absorbing solar radiation, whereas a concentrating collector focuses the sun's beam radiation to a smaller receiving area. Concentrating collectors usually have a concave surface and increased radiation flux compared to non-concentration collectors. Solar collectors can also be distinguished by the type of heat transfer liquid used and whether they are covered or uncovered by glazing. Another classification of solar energy collectors distinguishes between stationary, single-axis and two-axis tracking systems. (Kalogirou 2009, p. 121)

Stationary Collectors

Stationary Collectors are permanently fixed in position and do not follow the sun's movement. Therefore the collectors should be orientated directly toward the equator, facing south in the northern hemisphere and north in the southern hemisphere. The optimum tilt angle of the collector is equal to the location's latitude, with angle variations of 10° to 15°, depending on the application. The group of stationary collectors consists of three main types:

- Flat Plain Collectors (FPC)
- Stationary Compound Parabolic Collector (CPC)
- Evacuated Tube Collector (ETC)

Sun Tracking Concentrating Collectors

Energy delivering temperatures can be increased by sun tracking concentrating collectors. Very high temperatures can be reached if a large amount of solar radiation is concentrated on a small collection area. This is done by including an optical device between the source of radiation and the energy-absorbing surface. Many designs have been considered for concentrating collectors. Concentrators can be reflectors or refractors, can be cylindrical or parabolic, and can be continuous or segmented. Receivers can be convex, flat, cylindrical, or

concave and can be covered with glazing or uncovered. Concentration of the solar energy can be obtained by reflection or refraction of solar radiation by the use of mirrors or lenses. The reflected or refracted light is concentrated in a focal zone to increase the energy flux in the receiver. Due to the apparent movement of the sun across the sky, concentrating collector must be able to track this motion. Sun tracking concentrating collectors can be divided into following classes:

- Parabolic Trough Collector (PTC)
- Linear Fresnel Reflector (LFR)
- Parabolic Dish Reflector (PDR)
- Heliostat Field Collector (HFC)

The main parameter to consider the solar energy collector's quality is the thermal efficiency. It is the ratio of the useful energy delivered to the energy incident on the collector aperture. A common way to determine the thermal performance of a solar collector is experimental testing of prototypes under control conditions. In some countries the marketing of solar collectors is permitted only after testing procedures. (Kalogirou 2009, p. 219f)

2.3. Solar Radiation Models

The general challenge in the calculation of solar potential is the acquirement of solar radiation over an area of interest. Wong and Chow (2001) mention that the best database for the assessment of solar radiation would be the long-term measurement data at the site of the proposed solar system. Exact measurements are only possible for single locations, and not for a whole area of interest. Existing networks of solar radiation measurements are not dense enough to yield reliable values for a high spatial resolution, especially for areas that are far away from network stations. An interpolation has to be applied for large expanses. Another way to derive irradiance/irradiation values over a big area is the usage of meteorological geostationary satellites. This method yields less accurate values compared to ground measurements but has the important advantage of a satisfying coverage over vast territories. Thus, both techniques have drawbacks which lead to the development of solar radiation models. (Hofierka and Suri 2002)

Classification of Solar Radiation Models

Accurate prediction of the actual values of solar radiation for a specific location requires long-term average meteorological data which are still rare in underdeveloped countries. Therefore it is not possible to assess the solar radiation for every location in an accurate manner. Due to lack of data, meteorological parameters were estimated for the assessment of the solar irradiation maps in this thesis. Based on the employed meteorological parameters empirical models can be mainly classified into the four following categories (Besharat et al. 2013):

- **Sunshine-based models**: A widely used parameter to estimate global solar radiation is the sunshine duration. It can be easily recorded at weather stations.

- **Cloud-based models:** Clouds are among the most important weather phenomena restricting the availability of solar radiation on the Earth's surface. Cloud data is detected by meteorological satellites.

- **Temperature-based models:** Data about cloud distribution or sunshine duration is not available in all regions. Therefore many models use temperature measurements to predict solar radiation. The temperature-based models assume that there is a relation between the difference in maximum and minimum temperature and the faction of extraterrestrial radiation received at the surface.

- **Other meteorological parameter-based models:** Researchers have used many different meteorological parameters besides the already mentioned ones to predict the amount of global solar radiation.

2.4. Components of Solar Radiation

In a point on the top of the Earth's atmosphere the beam of incident sunrays is referred to extraterrestrial radiation (ETR). By passing through the atmosphere the ETR is attenuated and separated into three different components, namely the beam (or direct), the diffuse and the ground reflected radiation. The beam component of solar radiation is the part of ETR that directly reaches the Earth's surface without any atmospheric losses due to scattering or absorption (beam radiation). The sun's radiation that is scattered by air molecules, aerosol particles, clouds and other particles in the atmosphere is the diffuse component (diffuse radiation). Moreover the solar radiation that is reflected by the ground is also part of the total radiance (reflected radiation). (Paulescu et al. 2013)

While the assessment of the beam radiation is quiet straightforward and similar for different approaches the main difference between various models is the treatment of the diffuse component. The reflected radiation component usually has values of only several percent of the whole radiation and is therefore ignored in some models. Figure 2 illustrates a graphical sketch of the components of the solar radiation influenced by the Earth's atmosphere.

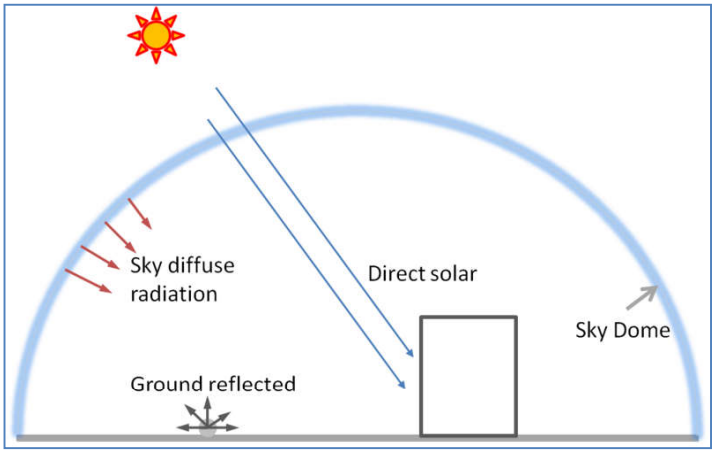

Figure 2: Components of solar radiation on the earth's surface (Vardimon 2011)

2.4.1. Beam radiation

Beam or direct radiation is the direct radiation that originates at the sun disk. Once the sun rays impinge on the Earth surface, the term radiation changes to irradiance or irradiation (see chapter 1.4.). The beam irradiance outside the atmosphere, also known as the solar constant accounts for 1366.1 W/m. Generally, the direct radiation is the largest component of total radiation (Fu and Rich. 1999). The irradiance falling on the earth's atmosphere changes

slightly over the year due to variations in the distance between the Earth and the Sun. All of the following quantities were published by Paulescu et al. (2013).

Normal beam Irradiance (G_n): G_n is the energy flux density (units: W/m²) of the solar radiation that reaches the earth surface in a 90° angle to the sun's rays (i.e. at an incident angle of 0°) without any atmospheric losses. Diffuse irradiation has no influence on this parameter.

Beam Horizontal Irradiance (G_b): The beam horizontal irradiance is the most important parameter to evaluate solar energy potential. It indicates the radiation energy on a horizontal plane on the earth's surface of the direct radiation. The energy flux density on a plane surface is directly proportional to the cosine of the incidence angle. Figure 3 depicts Austria's average annual sum of direct horizontal irradiance, considering the time period from April 2004 until March 2010. It is clearly recognizable that the southern and eastern parts have higher irradiation values than regions in the north and some areas in the mountains, especially in the north-eastern Alps. The formula to calculate the Beam Horizontal Irradiance is

$$G_b = G_n \cos(\theta_z)$$

where θ_z is the solar zenith angle, i.e. the solar incidence angle on a horizontal plane.

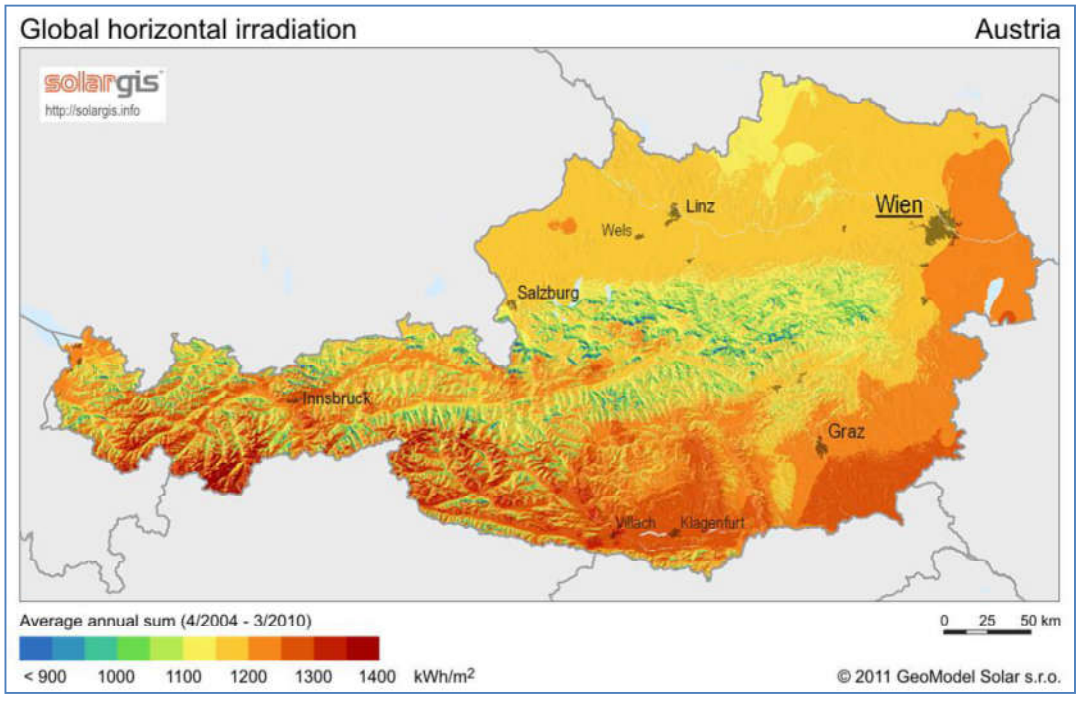

Figure 3: The averaged annual sum (4.2004 – 3.2010) of Austria's Global horizontal radiation (http://solargis.info/doc/free-solar-radiation-maps-GHI)

Inclined Irradiance (G_i): This quantity represents the Beam Horizontal Irradiance on an inclined surface. It is obtained by following equation,

$$G_i = G_n \sin(\delta)$$

where δ is the angle measured between the sun and an inclined surface.

2.4.2. Diffuse radiation

Diffuse radiation is the part of solar radiation that reaches the surface after scattering processes in the atmosphere. It is usually the second largest component of total radiation. Nevertheless, as the cloudless sky becomes more turbid, the diffuse irradiance increases and the beam irradiance decreases.

Diffuse horizontal irradiance (G_d) represents the energy flux density of the solar radiation incoming from the entire sky dome on a horizontal surface, except the direct beam coming from the sun's surface.

2.4.3. Ground reflected radiation

The ground reflected clear-sky irradiation (G_r) received on an inclined surface is proportional to the global horizontal irradiance (G, see later), to mean ground albedo and a fraction of the ground viewed by an inclined surface. This component accounts for a small proportion of total radiation and is therefore neglected for many purposes (Fu and Rich 1999).

Global irradiance (G) is the sum of the beam horizontal and diffuse components.

$$G = G_b + G_d = G_n cos\theta_z + G_d$$

The Total irradiance (G_t) is the sum of the beam horizontal irradiance, diffuse horizontal irradiance, and the additional flux density (G_r) reflected from the ground.

$$G_t = G_n cos\theta + R_d G_d + G_r$$

Where θ is the incidence angle and R_d is the conversion coefficient taking into account the sky view factor. The sky view factor is the extent of sky observed from a point as a proportion of the total possible sky hemisphere. It is dimensionless and has values between 0 and 1.

By summing up the irradiance over a finite time period one obtains the **solar irradiation** components:

$$\int_{t_1}^{t_2} G(t)dt$$

Optimum Angle (OPTA): The OPTA represents the angle of PV modules for maximum electricity production. The main parameter influencing this measure is the latitude of the site.

PV Electricity Yield (PVOUT): PVOUT is an estimation of the PV-system's electricity production.

Figure 4 depicts important angles for the assessment of large scale solar irradiation maps. They are classified in two groups: Angles that describe the Sun's position; Angles that describe the surface's position. The elevation angle is 90° minus the zenith angle and vise versa. The azimuth angle accounts for 0° towards south. All three angles for the position of the Sun are time dependent due to the changing position of the Sun in the sky. The angles that describe the position of the surface are steady over time. The surface normal is always perpendicular to the considered surface.

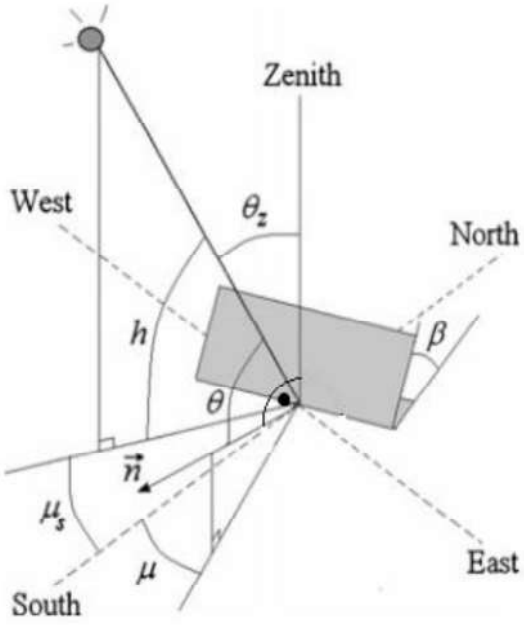

Figure 4: relevant angles for solar radiation (Paulescu 2013)

Angles describing the position of the sun:

$\theta_z = zenith\ angle$
$h = elevation\ angle$
$\mu_s = azimuth\ angle$

Angles describing the position of the surface:

$\beta = slope\ angle$
$\mu = surface\ azimuth\ angle$
$n = surface\ normal$
$\theta = angle\ between\ Sun\ and\ surface$

2.5. Solar Radiation Online Tools

In order to understand the variability of PV potential and estimate the electrical energy generated by a photovoltaic system, a number of online solar radiation tools have been developed. Two tools are discussed in this thesis.

2.5.1. PVWatts simulation tool

The National Renewable Energy Laboratory (NREL) developed the internet-accessible PVWatts simulation tool that estimates the electrical energy produced by a grid-connected crystalline silicon photovoltaic system. This tool uses Typical Meteorological Year (TMY2 by default) database and yield results for the area of the United States (Marion et. al. 2001). Users have the possibility to select a location and set PV system parameters, or keep default values, and PVWatts provides monthly and annual alternating current (AC) energy production in kilowatts per m² and energy values in dollars. PVWatts version 2 provides PV performance estimates by the use of 40-km resolution data grid values of monthly

- global horizontal radiation,
- direct normal radiation,
- and diffuse horizontal solar radiation.

Furthermore, values for monthly averaged daily maximum dry-bulb temperatures and monthly average surface albedo are considered in the data grid. Figure 5 shows the estimated annual alternating current (AC) energy production in kilowatts per m² and the energy value in dollars for a PV system size of approximately 25 m² in New York City. The default values were selected for each parameter.

RESULTS

Print Results

5,252 kWh per Year *

Month	Solar Radiation (kWh / m² / day)	AC Energy (kWh)	Energy Value ($)
January	2.62	284	66
February	3.63	347	81
March	4.74	487	113
April	5.30	510	118
May	5.51	530	123
June	6.38	581	135
July	6.30	584	135
August	5.74	538	125
September	4.94	459	107
October	4.02	404	94
November	2.87	282	65
December	2.31	245	57
Annual	4.53	5,251	$ 1,219

Figure 5: PVWatts results for a PV system of approximately 25 m² in New York City (http://pvwatts.nrel.gov/)

2.5.2. PV-GIS

Between 2001 and 2005 a European solar radiation database, called Photovoltaic Geographic Information System (PV-GIS) was developed using the solar radiation model r.sun (Suri and Hifierka 2004) and climatic data. This database consists of averaged global irradiation values and related climatic parameters of the period 1981 until 1990. PV-GIS has been used to assess the photovoltaic potential in the 25 EU (EU-25, 2004) member states and 5 candidate countries. The model estimates beam, diffuse, and reflected components of the global irradiation/irradiance for horizontal and inclined surfaces. The model's main input parameters were solar radiation, measured from 566 meteorological stations, atmospheric parameters and a digital elevation model (DEM). The resolution of the data grid is 1 km. (Suri et al. 2007)

The PV-GIS web tool uses the following equation to calculate the yearly potential of an installed PV system:

$$E = 365 * P_k * PR * G$$

Where E is the yearly electricity generation in kilowatt hours (kWh), P_k is the unit peak power in kilowatts (kW), PR is the system performance ratio, and G is the yearly sum of global irradiation on a horizontal, vertical or inclined plane of the PV module in kWh/m². (Suri et al. 2007)

Users can select a location in Europe and set several PV system parameters, such as used PV-technology, and PV-module's slope and azimuth. Since September 2014 PV-GIS also covers Africa and the western part of Asia (until 120° E) with a spatial resolution of 2 km. (http://re.jrc.ec.europa.eu/pvgis/).

3. MAJOR CHALLENGES

In order to assess the solar energy potential on roof areas for a region, two major problems have to be solved. Firstly, solar irradiation values have to be estimated and spread continuously over a certain area of interest. This can be done by interpolation methods, which have the big disadvantage of poor spatial resolution for large scale applications like cities. Therefore solar radiation models based on elevation raster maps are often used. These kind of models were already described in chapter 2.3. In the second step, the rooftop area has to be delineated from the residual part of the region of interest by means of various filtering methods. In the end, a conversion of solar radiation values in current electricity can be performed.

The basis of all calculations in this thesis is a LIDAR point cloud, recorded by airborne laser scanners. This chapter describes the main strategies to reach a solution for the problems of analysing the solar potential for an arbitrary test area based on former researches.

3.1. Solar Radiation Recording

The solar radiation received at the Earth's surface lies almost entirely in the wavelength band of 0,29 – 4 μm. Irradiance is the flux of short wave or solar radiation falling on unit area per unit time and is expressed as watts per square meter, abbreviated as W/m². Irradiation is the amount of solar energy falling on unit area over a stated time and is usually expressed as watthours per square meter per day or per year (Wh/m²/day, Wh/m²/year). Thus it is the integral with respect to time of the irradiance. Radiance refers to the short wave radiation received by the sky's scattering from a specific direction. (Page 1986)

A distinction of solar radiation recording methods can be justified with respect to the spatial resolution of the delivered data. In this context three recording types are distinguished. Solar radiation data acquired by airborne laser scanners have a fine spatial resolution but are in general not available for a global scale. The spatial resolution of ground measurements is bigger as it is of airborne methods due to interpolation between the stations of a network. In some regions of the earth, especially in developing countries, the network's distribution is neither uniform nor dense enough to yield accurate comprehensive values for solar radiation on the surface. The third recording method is performed by meteorological geostationary satellites.

3.1.1. Solar Radiation derived from airborne LIDAR measurements

Airborne LIDAR (**Li**ght **d**etection **a**nd **R**anging) recording systems are not able to measure radiation values directly. However, they are commonly used to generate Digital Elevation Models for a defined study area. These models serve as an input for various solar radiation models which estimate solar radiation throughout a region of interest. LIDAR data has the advantage of being available for many urban areas, with sufficient quality and density. Furthermore they contain relevant objects, like buildings and vegetation, to assess the solar radiation on a local scale. Their technology is based on a scanning laser in combination with a Global Navigation Satellite System (GNSS) receiver and internal technologies to yield three-dimensional point clouds. The scanner emits short laser pulses towards the Earth's surface and measures the round-trip times of the returning signals after diffusions and reflections on objects. The recorded round-trip times are directly related to distances from the sensor to the objects. Additionally, the direction of every laser beam is measured by the system and the single points are saved as polar coordinates which are transformed into national ground survey system coordinates. The transformation can be carried out using the flight path positions measured with a differential Global Positioning System (dGPS) and an Internal Measurement Unit (IMU). (Hollaus 2006)

3.1.2. Ground Measurements of Solar Radiation

Radiometers are used to measure the sun's electromagnetic radiation. It is possible to record every component of the solar radiation, described in chapter 2.4., with specific instruments. Details about those devices can be found in (Paulescu et al. 2013).

Even in developed countries networks for measuring solar radiation consist of relative small numbers of stations due to the high costs. This leads to the fact that the number of stations is too small to achieve accurate global coverage. Consequently, interpolation and extrapolation are applied to estimate solar radiation for each point of the Earth's surface. More than 1,000 globally distributed stations measure solar radiation. Cros and Wald. (2003) showed that daily solar irradiation may be considered valid in a 30 km circle around the measuring station. Even if these 1,000 stations were equally distributed over the whole earth less than 2% of land would be in the valid area. In other words, a big majority of the Earth would be too far away from the stations to deliver accurate information.

The largest global network measuring solar radiation is operated by the World Radiation Data Center (WRDC). The WRDC is located in St. Petersburg, Russia, and is part of the World Meteorological Organization (WMO). Solar radiation data is collected at more than 1,000 stations worldwide. The map in figure 6 represents the locations of the measurement sites on a global scale and shows the network's heterogeneity in regards to its spatial distribution.

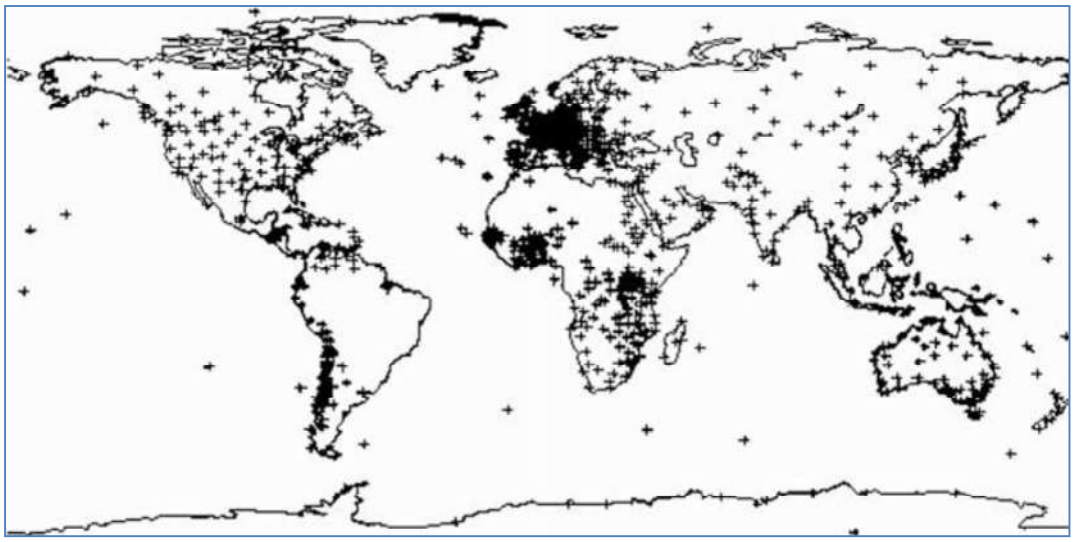

Figure 6: Distribution of the WRDC network (Paulescu 2013)

3.1.3. Solar Radiation derived from Satellite Observations

The sparse density and the heterogeneous distribution of ground stations yield the necessity to apply an alternative technique, such as satellite systems, to observe the solar radiation, especially on a global scale and on locations, which are far away from ground stations. Ground-based and satellite derived solar radiation data complement each other and are therefore necessary to develop global scale solar radiation databases.

Most of the methods that derive solar radiation from satellite observations take advantage of meteorological geostationary satellites that monitor the state of the atmosphere and the earth's cloud cover in the visible range in order to get estimations of the solar radiation at the Earth's surface. The geostationary satellites yield radiation data with a temporal resolution of 15 minutes and a spatial resolution of up to 1 km. Satellite-derived solar irradiation is the most accurate measurement technique for locations further away than 25 km from ground stations (Zelenka et al. 1999). Simple satellite models derive a cloud index to create a clear sky global irradiance model.

Vignola et al. (2007) compare satellite derived radiation values with ground measurements at specific stations of the University of Oregon Solar Radiation Monitoring Network. The

satellite derived values are obtained once every hour and represent a quiet large area (approximately 1 km²), whereas the ground data is based on the average of one point over one hour. This leads to a large variance in the datasets. However, with a perfect model the distribution of the differences should be normal and the averages should be the same. Perez et al. (2002) designed a satellite-to-irradiance model that aims to make a comparison possible.

3.2. Delineation of Rooftops

After finding an appropriate model to calculate the solar radiation it must be applied on a specific area. In the case of analysing radiation on rooftops, these areas have to be delineated and separated from the areas that are not of any interest for the further calculation steps. As mentioned before the basis of the calculations in this thesis is a 3-D point cloud of a test area recorded by an airborne laser scanner. Initially a Digital Surface Model (DSM) has to be generated. Based on this elevation model a Digital Terrain Model (DTM), that only represents the surface without any man-made objects or vegetation, is computed. In the end a classification of the whole area can be performed, based on different characteristics of the computed elevation model.

3.2.1. Generation of 3-D Elevation Models

In order to derive height features from the point cloud it is necessary to generate a Digital Terrain Model initially. Subsequently a normalized Digital Surface Model (nDSM) is calculated by subtracting the Digital Terrain Model (DTM) from the Digital Surface Model (DSM). Thus, the nDSM represents heights of all man-made objects and vegetation above ground. All outliers were removed a priori. In order to differentiate between points belonging and those not belonging to the ground, a variety of filtering methodologies can be performed. Some of the most important methods are listed below (Perez-Garcia et al. 2012).

Morphological Filtering: By using mathematical morphology operators, like erosion or dilation, non-ground elements, such as buildings and trees can be removed from the DTM. Vosselman (2000) introduces a distance-dependent slope threshold. This method is based on the observation that a large height difference between two nearby points is unlikely to be caused by a steep slope in the terrain. It is more likely that the higher point does not belong to

the ground. The probability that the higher point could be a ground point increases if the distance between the two points increases too. To express this assumption in a mathematical way, Vosselman (2000) defines the acceptable height difference between two points as a function of the distance between the points.

$$DEM = \left\{ p_i \in A \mid \forall p_j \in A : h_{p_i} - h_{p_j} \leq \Delta h_{\max}\left(d\left(p_i, p_j\right)\right) \right\}$$

A point p_i is a ground point if there is no other point p_j such that the height difference between these points is larger than the allowed maximum height difference at the distance between these points. Figure 7 shows the basic idea of a morphological filter with a maximum kernel size applied on a surface model. The allowed height difference between two points increases with the distance between the points. A point that is closer to another point of the DTM must not have a significant height difference to be a point of the surface model. The two basic morphological filters are dilation and erosion. Dilation generally increases the size of objects by filling internal holes and connecting pixels with small spaces in between. Erosion, in turn, decreases the size of objects and removes anomalies that are smaller than a specific radius. Erosion followed by a dilation is called opening and a dilation followed by an erosion is called closing.

Filter	Description
Dilation	Change pixel from '0' to '1' if at least 1 neighbourhood pixel is '1'
Erosion	Change pixel from '1' to '0' if at least 1 neighbourhood pixel is '0'

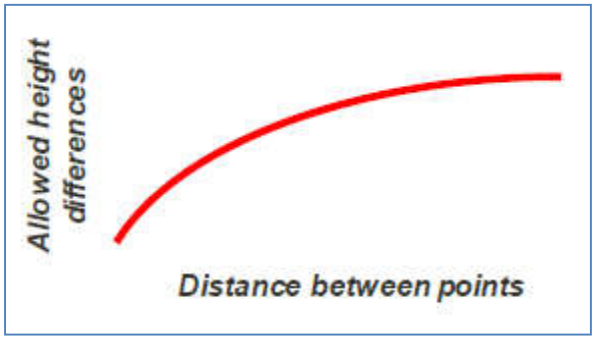

Figure 7: Basic idea of a morphological filter

Progressive Densification Filtering: The progressive approach starts with a small number of points to generate a first approximation of the surface. The procedure proposed by Axelsson (2000) begins with a triangulation process obtained from the lowest points presented in the area using a large grid size. Each iteration adds a new point to the Triangulated Irregular Network (TIN), if the point meets certain criteria (angle, distance) in relation to the triangle that surrounds it. The iteration process ends when there are no more points beneath the certain threshold.

Surface Based Filtering: Similar to the progressive densification filtering this method uses an initial surface approximation from a point cloud. It allows a computation of distances of the points to the surface model (residuals). If the point lies above the surface model it has less influence on the surface in the next iteration, and vice versa. The method proposed by Kraus and Pfeifer (1998) uses weighted linear least squares interpolation to iteratively approximate the ground surface. It is known as the robust interpolation method. The basic idea is that ground points usually have negative and off-ground points positive residuals. Thus a weight function was created that assigns high weights to the points with negative residuals and low weights to the points with positive residuals. Pfeifer et al. (2001) integrated this method in a hierarchical approach to handle large buildings and decrease computation effort.

3.2.2. Classification of Urban Areas

Urban landscapes belong to the most dynamic systems on earth. These areas consist of a big amount of different materials with specific characteristics. In other words, cities have a high spatial variance in every possible way. Thus an accurate classification of urban areas is a difficult task. For the assessment of the solar potential on roof areas only two classes are necessary. One class represents the pixels which are on roofs and the other class represents all other pixels in the raster map.

In the first step all points, which represent non-buildings areas – especially vegetation - have to be removed by applying a mask. This mask is generated by utilization of a certain threshold for the echo ratio values and heights for each pixel of the raster map. The echo ratio is a measure for local transparency and roughness and is derived for each laser point.

echo ratio [%] = n_{3D} / n_{2D} * 100.0

with $n_{3D} <= n_{2D}$

n_{3D} = Number of neighbours found in a fixed search distance measured in 3D (i.e. search sphere)

n_{2D} = Number of neighbours found in the same distance measured in 2D (i.e. vertical search cylinder with infinite height).

The echo ratio is close to 100% for flat areas, whereas the value decreases for rough areas. With increasing surface slope (e.g. steep roofs, walls) the echo ratio gradually decreases. To counteract this, the 3-D search radius has to be extended in respect to the local surface slope. This is done by dividing the initial 3-D distance by the cosine of the surface slope. Figure 8 depicts the point cloud based calculation of echo ratio for each laser point with example values of different objects. In addition it shows the slope adaption depending on the local surface slope.

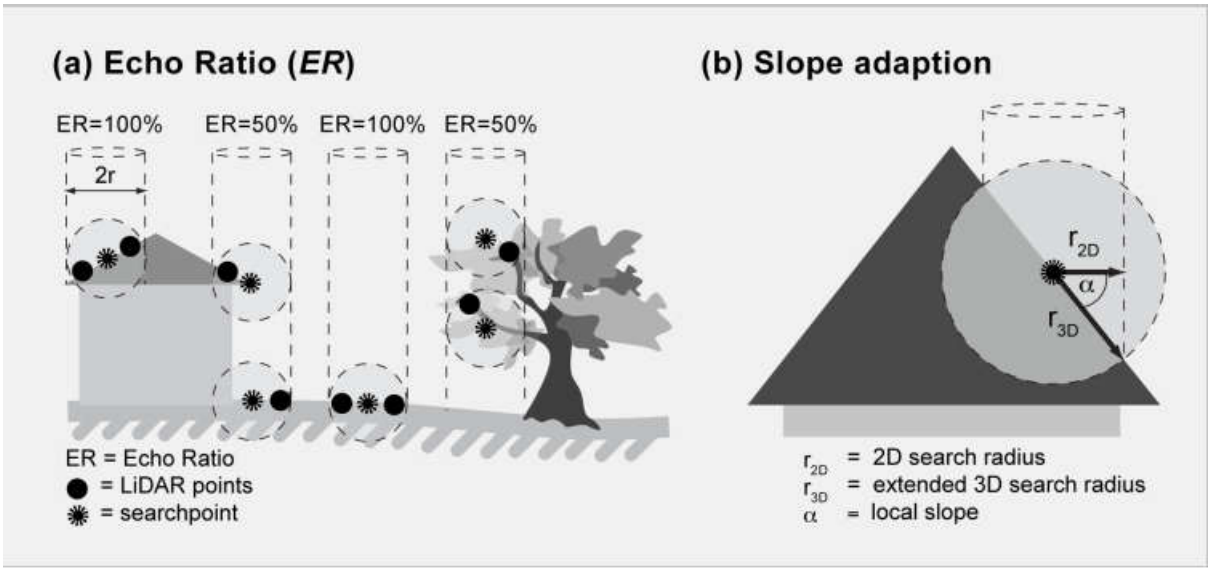

Figure 8: a) Assessment of echo ratio value for single laser points of a point cloud; b) slope adaption depending on local surface slope (Höfle et al. 2009)

Additionally, the mask has to consider DSM heights and eliminate all low points by a segmentation based on a height threshold. A reasonable value for the threshold could be between 3m and 4m according to Yu et al. (2010). If the value is too high, the algorithm will delete many pixels which represent low off-ground points, which could be building points. If the value is too low, some small objects will be mistakenly detected as buildings. In this thesis a threshold of 5 meters above ground is applied I the process of generating a mask. It is very

likely that the resulting binary map (mask) contains some artefacts which can be removed by morphological filters.

4. METHODS

This chapter addresses the practical approaches of the solar potential calculation for a specific test area. The test area's solar potential is assessed by three different methods applied by different calculation programs. Despite the method, a model of the entire roof area has to be created based on a point cloud recorded by an airborne laser scanner.

4.1. Test Area and Data

A part of the 9th district of Vienna, Austria, was chosen for the study (see figure 9). The area's centre is approximately at 48.21° N and 16.35° E and has mainly residential characteristics. Furthermore it includes a small park with high trees that could cause problems with shadows in the calculation of solar irradiance. The majority of the roofs is pitched and tilted towards the closest street. The raw data is a three-dimensional point cloud acquired by an airborne laser scanner. The mean value of the point density is 29.69 points/m² and the standard deviation is 17.08. Figure 10 depicts a histogram of the point cloud's point density.

Figure 9: Test area in the 9th district of Vienna (extract from maps.google.com)

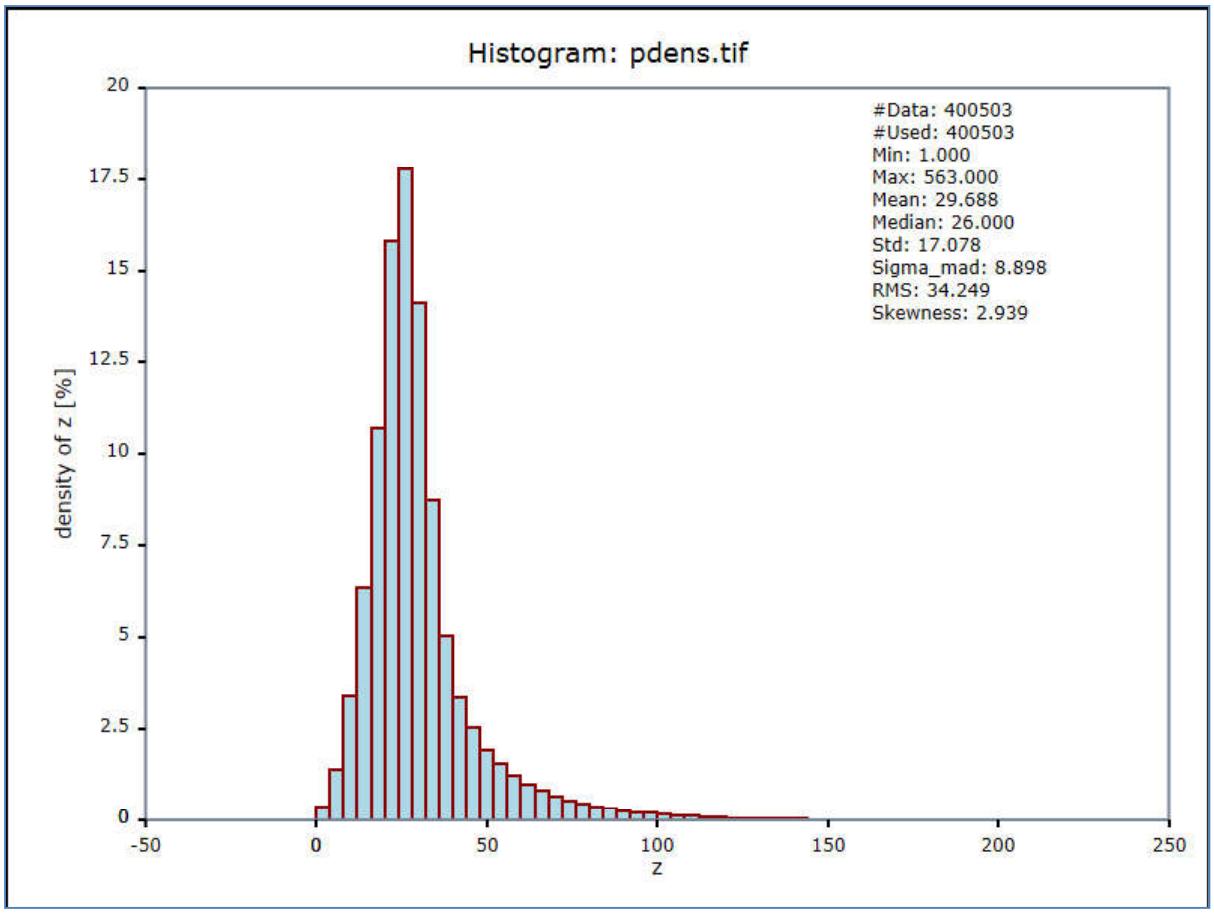

Figure 10: Histogram of the distribution of the point density (laser points per m²): The x-axis represents the amount of points per m² in the test area. They are classified in groups due to their point per m² value and visualized as bars in this histogram. The y-axis depicts the percentage of appearance of each class.

4.2. Generation of a Roof-filtered Irradiation Map

To create a map that represents only the roof areas of a region a classification of the LIDAR points has to be done. In this classification only two classes are necessary: roofs and no roofs. The basic idea is to find the locations of the rooftops by taking advantage of the fact that these areas show specific characteristics which other areas do not have. The software **OPALS** (Pfeifer et al. 2014), developed at the Technical University of Vienna, is used to calculate the classification for this study. Standard LiDAR sensors are capable to acquire 3D topography data in urban areas with sufficient density.

In the first step a Digital Surface Model (DSM) is generated based on a three-dimensional point cloud. Then a Digital Terrain Model (DTM) is calculated. By subtracting the DSM with the DTM a normalized Digital Surface Model (nDSM) is processed. All the models have a pixel size of 25 x 25 cm². The nDSM is representing the heights of the single points in the

point cloud in respect to the DTM. In the next step a classification is performed by considering the nDSM heights and the echo ratio of the 3-D-model. The threshold for the height of roofs is set to a value of 5 meters. Therefore an area can only be assessed as a rooftop as long as its height difference from the ground accounts for 5 meters or more. By looking at the echo ratio map it becomes clear that flat surfaces like roads and roofs have higher values than rough surfaces such as vegetation. Also edges of buildings, roof ridges and very steep roofs are represented by a low echo ratio. A certain threshold is used to distinguish between rough and smooth surfaces. Once appropriate thresholds are found morphological filtering is applied to yield an adequate mask for roof areas. Raster points of the nDSM that are 5 meters or higher above the ground and smooth will be classified as roofs. Figure 11 shows the echo ratio separated in 5 classes. The green areas are mostly trees and other vegetation or edges of buildings. The brown areas depict mainly roofs and streets.

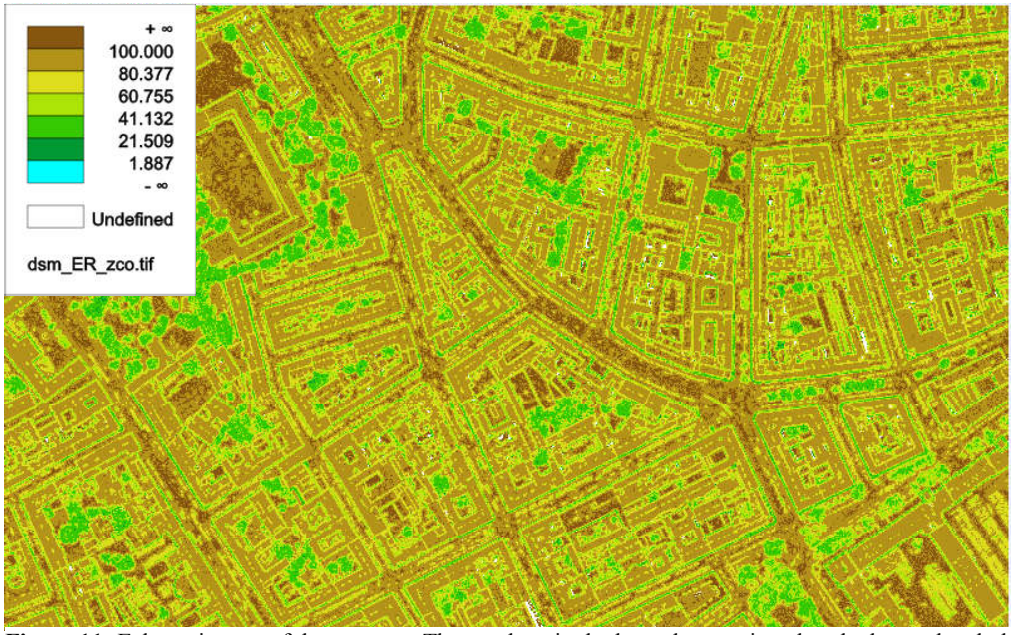

Figure 11: Echo ratio map of the test area: The numbers in the legend are assigned to the lower threshold of the classes. That means for the class that is visualized in dark green: The range of this class is 1.887 until 21.508. 21.509 is the lower threshold of the next class.

Figure 12 shows the workflow in order to obtain a roof filtered mask. By processing the point cloud in OPALS, two results are obtained: A DSM and a DTM, representing the surface in a 3-D-model. The difference of these two raster maps yields a so called nDSM. The roof map is assessed by applying the thresholds for the height and echo ratio on the nDSM.

In the following three flowcharts blue boxes represent calculation results and green boxes processing steps.

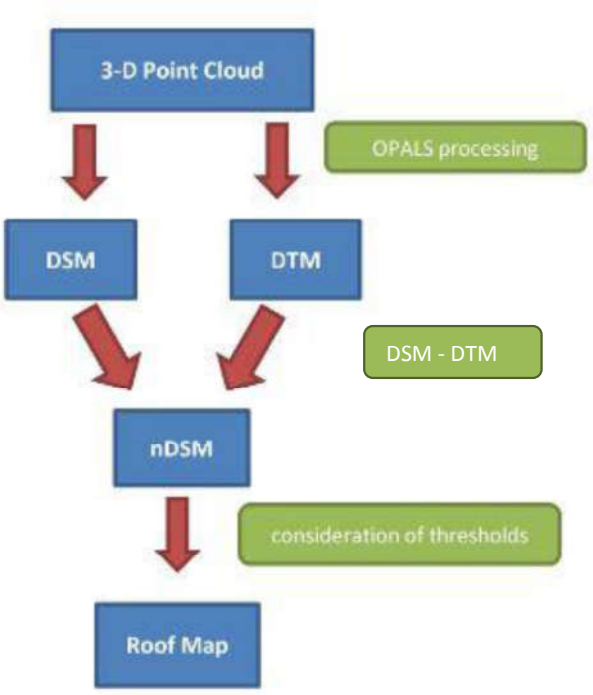

Figure 12: Flowchart, describing the generation of a roof map

4.3. Calculation of the Solar Potential Map

The result of chapter 4.2 is a raster file that visualizes the extent of the rooftop areas. In the rooftop mask the value 1 is allocated to all pixels which are classified as roof areas, and all pixels that are located outside the rooftops have the value zero.

Prior to the application of the different methods, the influence of the vegetation has to be analysed, in order to decide on the topographic model as a part of the input. Figure 13 shows the approach of analysing the vegetation's influence in the test area. The solar radiation over the whole year has to be calculated, due to the varying shadow geometry for the 3-D-models. This can easily be performed by the Solar Analyst in the program in ArcMap. At first the objects outside the rooftop areas are included in the solar irradiation calculations (DSM), then they are excluded (Rooftop DSM). In the second step the rooftop areas are masked out by pixel-wise multiplications of the maps with the pixels of the roof mask. Thus only solar irradiation values for buildings remain and a comparison of the maps is possible by computing their difference – again in a pixel-wise manner.

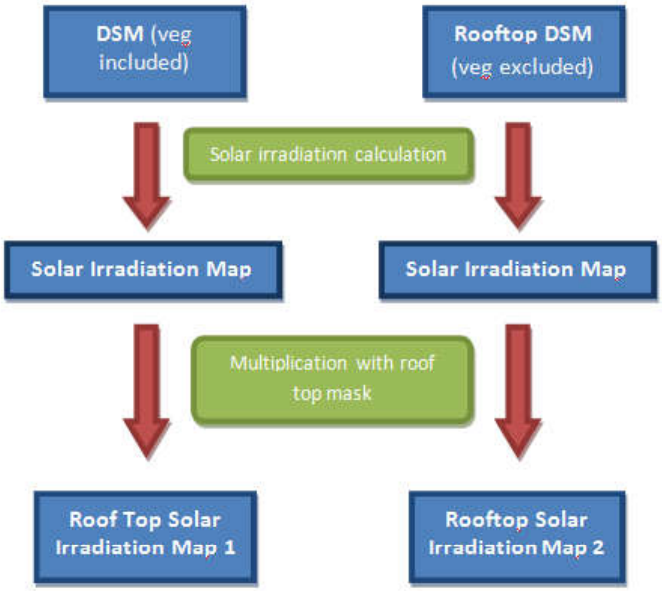

Figure13: Analysis of the vegetation's influence

The estimation of the solar potential map for roof areas is executed by three different programs including commercial software (ArcGIS/ArcMap, www.esri.com), a freeware (QGIS, www.qgis.org), and a program that is still in its development phase (VOSTOK). Thus the distinction in the methods is only present in this processing step. In this thesis solar potential maps are only assessed for four special days of the year 2015. These days are the two equinoxes, which occur around the 21st of March and the 23rd of September, the winter (21st of December) and the summer solstice (21st of July). After calculating the solar irradiation maps based on an elevation model, the resulting raster maps are multiplied by the roof mask raster map by means of a raster calculation tool. This step is necessary to delete all irradiation values outside the areas which are classified as rooftops. Figure 14 demonstrates the general procedure of estimating a solar irradiation map for roof areas only.

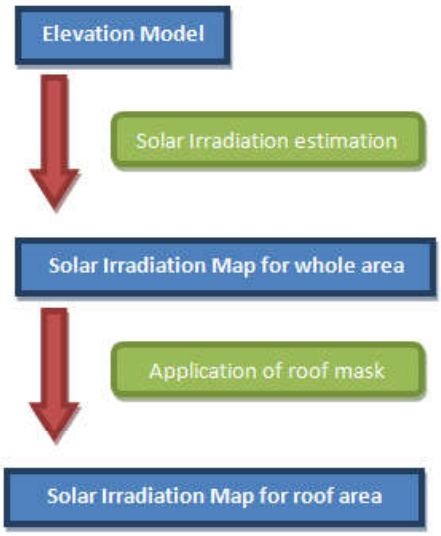

Figure 14: Assessment of a solar irradiation map for roof areas only

As described in chapter 3.2 the solar radiation can be divided into three individual components: The direct (or beam), the diffuse, and the ground reflected part. The majority of models neglects the ground reflected part due to its small quantity and its sophisticated handling.

4.3.1. ArcMap's Solar Potential Map

Esri's ArcMap is a program that enables geospatial processing for raster and vector files. It offers two methods to perform a solar radiation analysis within the Solar Analyst tool:

- **Area solar radiation analysis** is used to calculate solar radiation across a specific region. The calculations are repeated for each location (each raster point) of the topographic surface, producing insolation maps for the entire area.
- **Point solar radiation analysis** is used to calculate the solar radiation for a given location only.

For the application of this study, where the assessment of the solar radiation for an entire landscape that is represented by the test area, is the declared goal, only the area solar radiation analysis is relevant and will be discussed in detail in this chapter.

The Area Solar Analyst extension calculates insolation maps using digital elevation models (DEMs) as input. The local effect of topography is considered by means of upward-looking

hemispherical (fisheye) photographs for each point of interest on a DEM (Rich, 1989). These viewsheds result in radiation values for each location and produce accurate insolation maps. The solar radiation tools in Spatial Analyst do not include ground reflected radiation in the calculation of total radiation. Therefore, the total radiation is calculated as the sum of the direct and diffuse radiation (ArcGIS Online Help).

Three raster representations of the sky are calculated for every location of interest:

- Viewshed
- Sunmap
- Skymap

The viewshed is a representation of the entire sky that is visible or obstructed when viewed from a particular location. The calculation is performed by determining the maximum angle of sky obstruction for a specific number of directions around the location of interest. For the directions in between, the horizontal angles are interpolated. All horizon angles are then converted into a hemispherical coordinate system that represents a three-dimensional hemisphere of directions as a two-dimensional raster image. Figure 15 shows the process of generating a hemispherical viewshed for a point of a DEM.

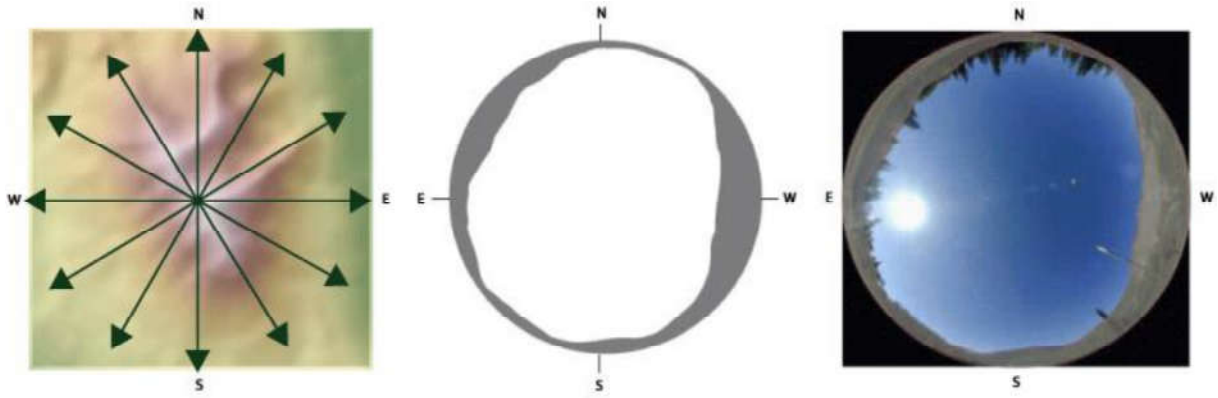

Figure 15: Calculation of a hemispherical viewshed for one point of a DEM; left: Visualization of the terrain around the point. Centre: Viewshed for this point. Right: vertical fisheye photograph

The sunmap calculates the direct solar radiation in the same hemispherical projection as the viewshed. It is a raster representation that depicts the sun track for a specific location through the hours of a day or the days of a year and consists of discrete sectors defined by the sun's position. The sun track varies for different latitudes and time configurations.

Diffuse radiation originates from all sky directions as a result of scattering by the atmosphere. The **skymap** is created to calculate diffuse radiation for a particular location. It represents a hemispherical view of the entire sky divided into sectors similar to the sunmap.

During the calculations the viewshed raster is overlaid with the sunmap and skymap rasters to calculate the direct and diffuse component of the sun's radiation from each sky direction. Thus the calculation of an insolation map is performed in four steps:

- Calculation of an upward-looking hemispherical viewshed
- Overlay of the viewshed on a direct sunmap
- Overlay of the viewshed on a diffuse skymap
- Repeating the process for every location of interest

4.3.1.1. Model Inputs

The main input for the area solar radiation analysis is a DEM of the investigated region. To include the latitude information one integer value is defined for the whole area. With large datasets (i.e. states, countries or continents) the insolation results will differ significantly at different latitudes. Therefore it is crucial to divide big study areas into zones of different latitudes. Another parameter that is important for the calculation of solar radiation is the time span. The maximum time span is one year for multiple-day time configurations and one day for within-day configurations. The default day interval for multiple-day calculations is 14 days and the default hour interval for single days is 30 minutes. Skysize is the resolution of the viewshed, skymap and sunmap rasters which are used in the radiation calculations. These are upward-looking, hemispherical raster representations of the sky and do not have a geographic coordinate system. Increasing skysize enhances the accuracy but at the same time also increase the calculation time. The maximum skysize value is 4000 (200 by default).

Table 3 lists the most important input parameters. To see the complete table go to: http://webhelp.esri.com/arcgisdesktop/9.2/index.cfm?TopicName=Area_Solar_Radiation.

Parameter name	Type of input	Description
in_surface_raster	Raster	Input DEM surface raster
latitude	Single value	Latitude for the site area (units: decimal degrees)
sky_size	Single value	resolution for viewshed, skymap and sumap grids
time_configuration	Time configuration	Time period used for calculations
day_interval	Single value	Time interval through the year
hour_interval	Single value	Time interval through the day

Table 3: Important input parameters for ArcMap Solar Analysis

4.3.1.2. Model Outputs

The output global radiation raster contains float values and renders solar radiation with units of watt hours per square meter (Wh/m²). In addition direct and diffuse solar radiation maps and direct incoming solar radiation duration raster maps can be calculated.

Parameter name	Type of input	Description
out_global_radiation_raster	Raster	Global radiation raster file (direct + diffuse)
out_direct_radiation_raster	Raster	Direct radiation raster
out_diffuse_radiation_raster	Raster	Diffuse radiation raster
out_direct_duration_raster	Raster	Direct incoming solar radiation raster (units: hours)

Table 4: outputs of the area solar radiation analysis in ArcMap

4.3.1.3. ArcMap Model

Figure 16 shows the processing model of ArcMap in a simplified depiction. In order to perform a solar irradiation calculation for a test area, two kinds of parameters have to be defined, in addition to an elevation model (DSM). These parameters are grouped in two classes: atmospheric and temporal parameters. Atmospheric parameters are called Transmittivity and Diffuse Proportion and their default values and range are described in table 9, chapter 4.4. The number of the day of the year, the time step of interpolation and the year of calculation are the content of the temporal parameter class.

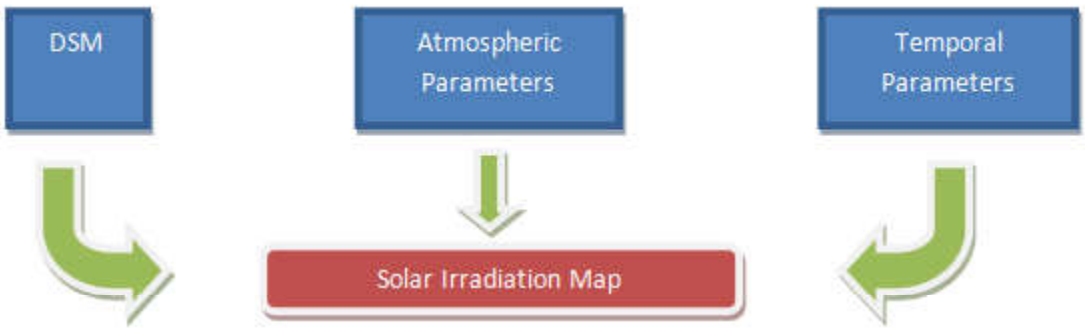

Figure 16: ArcMap Processing Model

4.3.2. QGIS's Solar Potential Map

Analysing the solar potential with QGIS is performed with the GRASS extension "Solar irradiance and irradiation model" (r.sun). The r.sun model works in two modes. **Mode 1** calculates a solar incidence angle in degrees and solar irradiance values (Wh/m²) for the instant time. **Mode 2** yields the daily sum of solar irradiation (Wh/m²/day) and duration of the beam irradiation within a defined day. (Hofierka and Suri 2002) Based on clear-sky conditions r.sun computes direct (beam), diffuse and reflected solar irradiation raster maps for a given day, latitude, surface and atmospheric conditions. Direct, diffuse and reflected radiation are the three components of global radiation. As an option the model considers a shadowing effect of the local topography. Various solar parameters are saved in a history file. Besides a raster file that represents the elevation for every pixel other parameters have to be defined for the model.

The theoretical basis of the model arises from the development of European Solar Radiation Atlas. The implemented equations for diffuse radiation in r.sun represent especially European climate conditions. Therefore higher estimation errors in diffuse models are expected for regions outside Europe. Unlike the ArcMap model, r.sun delivers a solution for calculating the ground reflected component of solar radiation.

4.3.2.1. Model Inputs

Mandatory input files besides the elevation map are the slope and aspect map of the analysed area in both modes. In addition, mode 1 requires local solar time information and mode 2 needs information about the day of the year. (Hofierka and Suri 2007)

Parameter name	Type of input	Description	Mode
elevin	raster	Elevation raster map	1,2
aspin	raster	Aspect raster map	1,2
slopein	raster	Slope raster map	1,2
day	single value	No. of day of the year	2
time	single value	Local (solar) time	1

Table 5: Mandatory inputs for r.sun (Hofierka and Suri 2002)

Slope and aspect of the DSM, which was obtained from a point cloud, described in chapter 4.2., are calculated with raster based terrain analysis techniques which are performed by means of the raster terrain analysing plugin in QGIS. The slope calculation tool renders the slope angle for each cell in degrees. The aspect tool calculates the aspect of each cell in degrees in a counter-clock-wise manner starting with zero for north direction. However, the fact that the r.sun tool considers 0° or 360° degrees as west for its computation, makes an adaption of the raster map essential. A counter clockwise rotation of 90° degrees has to be conducted before including the aspect map in the process of estimating solar irradiation values for each pixel of the test area.

In mode 2 the solar radiation maps are computed by integrating the relevant irradiance between sunrise and sunset for a given day. The default value of the time steps is 30 minutes. There is no need to define the latitude for locations with known projections or coordinate systems. In this study the solar potential was computed for several days.

4.3.2.2. Model Outputs

The outputs for mode 1 are the solar incident angle and three solar irradiance raster maps, which visualize the beam, diffuse and reflected component of solar radiation. Calculations in mode 2 also give three raster maps that represent the sum of solar irradiation within a given day. In addition a raster map showing the duration of beam irradiation can be displayed. Table 6 shows the outputs for mode1 and table 7 the outputs for mode 2 respectively.

Parameter name	Description	Unit
incidout	solar incidence angle	Decimal degrees
beam_rad	beam irradiance	W/m²
diff_rad	diffuse irradiance	W/m²
refl_rad	reflected irradiance	W/m²

Table 6: r.sun outputs for mode 1 (Hofierka and Suri. 2002)

Parameter name	Description	Unit
insol_time	duration of beam irradiation	Minutes
beam_rad	beam irradiation	Wh/m²*day
diff_rad	diffuse irradiation	Wh/m²*day
refl_rad	reflected irradiation	Wh/m²*day

Table 7: r.sun outputs for mode 2 (Hofierka and Suri 2002)

Besides output raster maps the model stores basic solar radiation parameters, like sunset and sunrise times, in a text file.

4.3.2.3. QGIS Model

The model to assess the solar irradiation of a test area in QGIS is similar to the ArcMap model. It is visualized in figure 17. The DSM and the temporal parameters are the same in ArcMap. The Atmospheric Parameter is called Linke atmospheric turbidity (Linke F. 1922). The ground reflecting component of solar irradiation is included in the algorithm of QGIS additionally and can be influenced by the Albedo parameter. Thus it is a topographic parameter. The two mentioned parameters that can be modified are described in detail in chapter 4.4. In addition to the albeldo value, slope and aspect values for every pixel of the DSM also account for topographic parameters. QGIS offers the possibility to calculate them before the solar irradiation computation is performed.

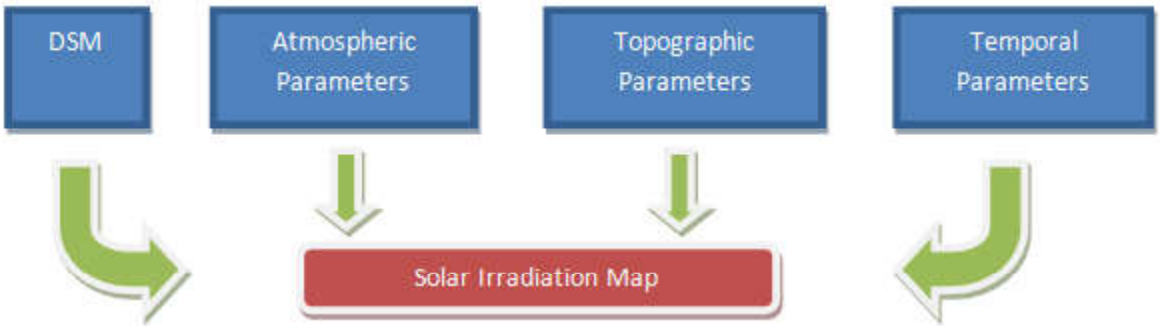

Figure 17: QGIS Model to obtain a solar irradiation map

4.3.3. VOSTOK's Solar Potential Map

VOSTOK (Voxel Octree Solar Toolkit) (Jochem et al. 2011) (Jochem et al. 2009) is a C++-Program for calculations of the solar potential of a region based on point clouds. Contrary to ArcGIS and QGIS, VOSTOK is conducted over the command prompt. An ASCII-file with the extension .sol that includes all important input parameters for the calculation of the solar radiation has to be created.

4.3.3.1. Model Inputs

VOSTOK requires an ASCII-formatted raster file as an input surface model (Bechtold 2015). This file has to contain the x, y and z values and their normal vector components in every direction for each raster cell. All parameters that are necessary to perform the calculation are defined in the before mentioned .sol-file. VOSTOK offers the possibility to determine a shading point cloud and a solar radiation point cloud individually. Another parameter is the point cloud's projection to obtain its location on the earth. The time period for the assessment is entered through the starting and end time and its maximum value is one year. The intervals can be defined for multiday- or daily-configurations.

Parameter	Description
Shading point cloud	Point cloud in .xyzn
Solar radiation point cloud	Point cloud in .xyzn
Projection	Projection (PROJ4) for both point clouds
Voxel size	Voxel size in meter
Year	Calculation year (relevant for leap year)
Starting day	Day of the year to start the calculation
End day	Day of the year to end the calculation
Day interval	Daily interval for multiple-day applications
Hour interval	Hourly interval for within-day applications
Calculation shadows	Flag to consider shadows

Table 8: Important input parameters for VOSTOK

4.3.3.2. Model outputs

The name of the output file has to be defined in the .sol-file. The result is an ASCII file that contains 2-D-coordinates for each pixel and their solar radiation value.

4.3.3.3. VOSTOK Model

VOSTOK uses a rather straightforward model to calculate a solar irradiation map. Except for the Digital Surface Model (DSM), only temporal parameters are needed to conduct the estimation over the test area. Unlike the other two considered programs, VOSTOK does not deliver the possibility to change atmospheric or surface parameters.

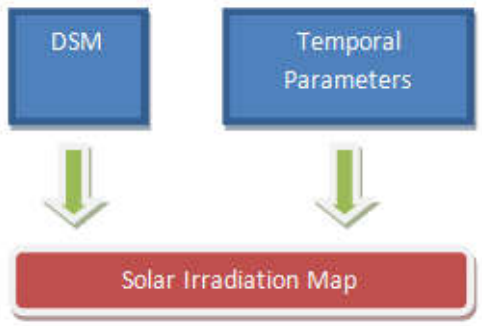

Figure 18: VOSTOK Model to estimate a solar irradiation map

4.4. Comparison of the methods

In general, the programs described above apply different methods and require various input parameters to assess the solar irradiation for each pixel of a specific area. Besides the already mentioned inputs, ArcMap and QGIS offer the possibility to edit input parameters, which influence the incoming solar irradiation on the Earth's surface. These variables are discussed in table 9, on the following page.

An accurate and reliable solar potential analysis requires calculations of solar irradiation over the whole year, due to the annual movement of the Sun relative to every location on the Earth. In order to reduce the processing time, only daily maps are assessed in this thesis. Since the goal is to obtain a relative comparison of the different programs it is sufficient to analyse daily irradiation values.

All three programs calculate the solar irradiation based on a three-dimensional elevation model. In the case of analysing rooftops, this model is a high resolution Digital Surface Model (DSM) with a pixel size of 25 x 25 cm² for the requested urban area. The pixel sizes of the resulting maps are also 25 x 25 cm² in the case of ArcMap and QGIS solar irradiation calculation, whereas VOSTOK outputs a raster map with a minimum pixels size of 1 x 1 m². Thus VOSTOK's irradiation map has a lower resolution than the maps which are obtained by the other two programs.

Topographic parameters that have an influence on the solar irradiation performance of an arbitrary surface are the surface's slope and aspect. QGIS requires a computation of these two parameters for each pixel of the DSM a priori. The results of these computations are raster maps. As discussed in chapter 4.3.2.3 QGIS includes the ground reflected component of solar irradiation in its solar potential assessment. Thus the algorithm contains another parameter to describe the topography of the elevation model. It is called albedo and quantifies the reflection ability of a surface. VOSTOK and ArcMap retrieve slope and aspect values automatically from the DSM and include them in their calculations. VOSTOK supplies the possibility to define a three-dimensional model that accounts for the shading effects and another model that serves as the solar irradiation surface individually.

Parameters, describing the atmospheric condition and surface characteristics, can only be edited in ArcMap and QGIS. These two programs use different parameters in the calculation of the solar irradiation. ArcMap only includes atmospheric parameters which are called transmittivity and diffuse proportion in the processing. Both parameters have values between

0 and 1. The transmittivity is the fraction of the radiation that passes through the atmosphere (averaged over all wavelengths). The parameter called diffuse proportion represents the proportion of global normal radiation flux that is diffuse. (ArcGIS online help) The editable atmospheric parameter for QGIS is called Linke Atmospheric Turbidity. The albedo value represents a surface parameter that can be modified. Values for Albedo range from 0 to 1 and express a measure for reflexion of the Earth's surface. The Linke Atmospheric Turbidity has values from 1 until around 8. It is a convenient approximation to model the atmospheric absorption and scattering of the solar radiation under clear skies. Thus it describes the optical behaviour of the atmosphere due to two aspects: The absorption by the water vapour and the absorption and scattering by the aerosol particles in relation to a dry and clean atmosphere. In other words, it summarizes the attenuation of the direct solar radiation. (Angles J. et al. 1999) Table 9 shows all editable parameters and their default values and bandwidth in the particular program. At this point it is important to mention that all parameter are dimensionless quantities.

ARCMAP			**QGIS**		
Parameter	**Default value**	**bandwidth**	**Parameter**	**Default value**	**bandwidth**
Transmittivity	0.5	[0 1]	**Linke Atmospheric Turbidity**	3.0	[1 8]
Diffuse proportion	0.3	[0 1]	**Albedo**	0.2	[0 1]

Table 9: Editable atmospheric and surface parameters

5. RESULTS AND INTERPRETATION

This chapter refers to the results of the solar irradiation processing. In addition to the processing of the data, a series of statistical analysis is performed to compare the results of the different calculations with each other.

The rooftop area of the test region consists of 2,979,997 pixels. Each pixel has 625 cm² (25 x 25 cm²), thus the rooftop area has an extent of 186,249.81 m². The size of the whole test area is 400,325.06 m², which is equal to 6,405,201 pixels. Thus the percentage of rooftop area is 46.52% for the considered region of the 9th district of Vienna.

VOSTOK was not able to conduct a solar irradiation assessment over the whole test area. Only the irradiation values for a fraction of the whole region are obtained. Therefore a subset of the whole test area, where all three programs yield reliable results, is used for further statistical analysis and comparison. The selected subset for further investigations has an extent of 59,748.75 m². Its rooftop area is 33,046.00 m² (55.31%).

The solar irradiation maps over the subset area for three special days are calculated. These days are the two equinoxes, which occur around the 21st of March and the 23rd of September, the winter (21st of December) and the summer solstice (21st of July). Table 10 outlines statistical results of the solar irradiation map for the 21st of March, calculated with VOSTOK. The resulting text file contains 1,048,576 entries. That leads to an expansion of 65,536 m² that is only 16.37% of the total test area.

Mean [Wh/m²/day]	3,582.38
Maximum [Wh/m²/day]	7,359.37
Minimum [Wh/m²/day]	334.10
Standard deviation [Wh/m²/day]	1,681.58

Table 10: Statistical measures of the solar irradiation map, calculated with VOSTOK (21st of March)

5.1. The Influence of Vegetation

As mentioned in chapter 4.3, in the first step of assessing the solar potential of the test area, two annual solar irradiation maps are calculated by the same program (ArcMap) to investigate the vegetation's influence on the solar irradiation performance. In the calculation of solar irradiation map 1 the vegetation is included, as a potential source of shadows on roofs. Solar irradiation map 2 excludes all objects outside rooftop areas for the computation. The comparison of both maps shows that the differences between the two solar radiation maps are significant in some areas. For the chosen test area the vegetation changes the solar radiation values in a substantial way. Therefore it is necessary to consider objects outside of rooftops for the calculation of the solar potential of the given test area.

Statistical measures of the two raster maps are presented in table 11. Although the comparison of the two maps yields similar results, there are regions where the influence of the vegetation on the solar irradiance on roofs is significant.

Raster map	**Vegetation included**	**Vegetation excluded**
Mean value [kWh/m²/year]	734,757	736,339
Maximum Value [kWh/m²/year]	1,153,620	1,153,030
Minimum Value [kWh/m²/year]	11	32
Standard Deviation [kWh/m²/year]	285,307	289,770

Table 11: Results of statistical calculations of the annual (2015) irradiation maps

Figure 19 and 20 visualize the high difference in annual solar irradiation in an extract of the test area, performed in ArcMap by application of raster calculations. In this extract the vegetation's density is higher, compared to the rest of the test area. Thus the trees are supposed to influence the solar irradiation performance more severely. Figure 19 displays the solar irradiation values, which are calculated without any influence of objects outside of the rooftop area. These objects – mostly trees – are included in figure 20. Dark red pixels represent high solar irradiation performance and light red pixels show low irradiation values, respectively. Due to the shadow causing trees, some locations yield smaller irradiation in the map that considers objects outside of roofs as potential obstacles. This observation is emphasized through green circles in figure 20.

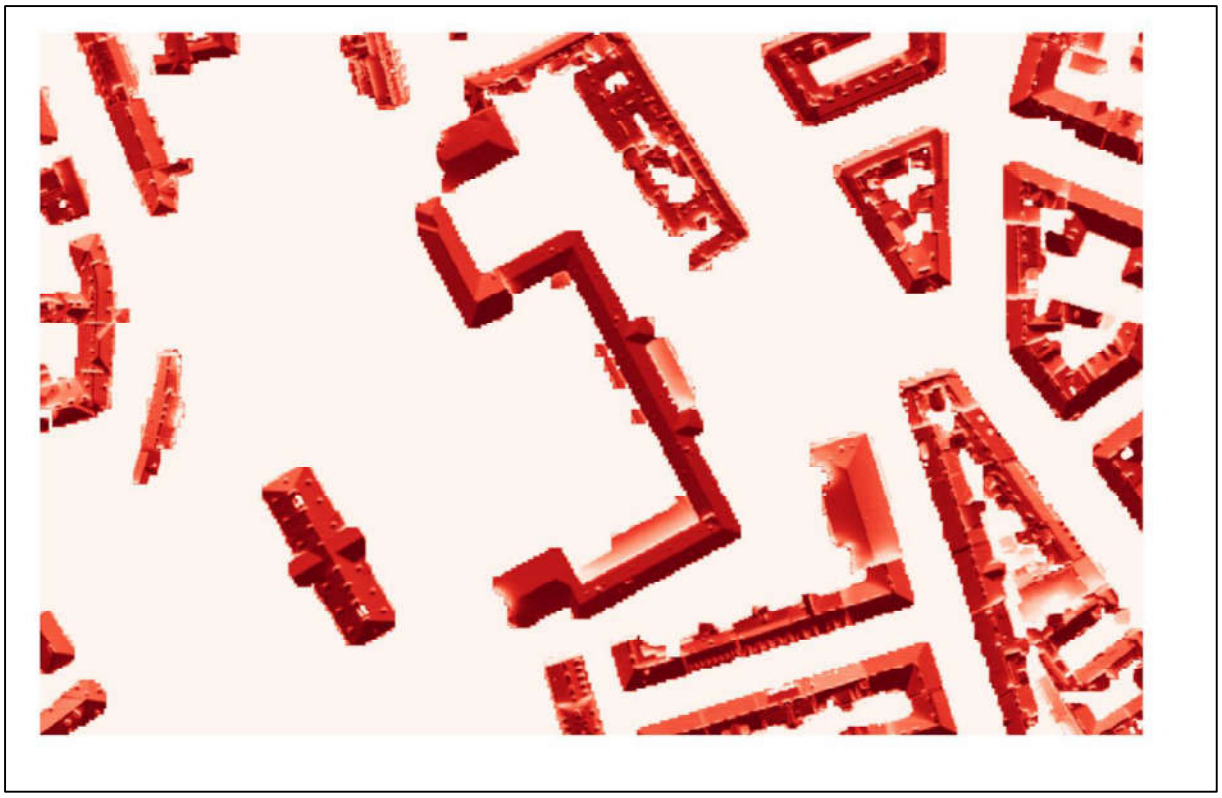

Figure 19: Solar irradiation map without any influence of objects outside the rooftop area

Figure 20: Solar irradiation map with the influence of objects outside of the rooftop area

Figure 21 has the same extent as the maps above and depicts high differences in pink between map 1 and map 2, overlayed on the DSM. The pixels with the highest 10% of the difference map are classified as high differences in the visualization. In the DSM bright gray-scale values indicate high and dark values low elevation. The distribution of vegetation can be clearly seen, due to their random geometry. All man-made objects, such as buildings, are characterized by simple geometric structures, which mainly are straight lines and large angles. After optically analyzing the raster map the assumption is made, that low buildings, which are close to high trees, are very likely to experience a significant influence by other objects than neighbouring buildings.

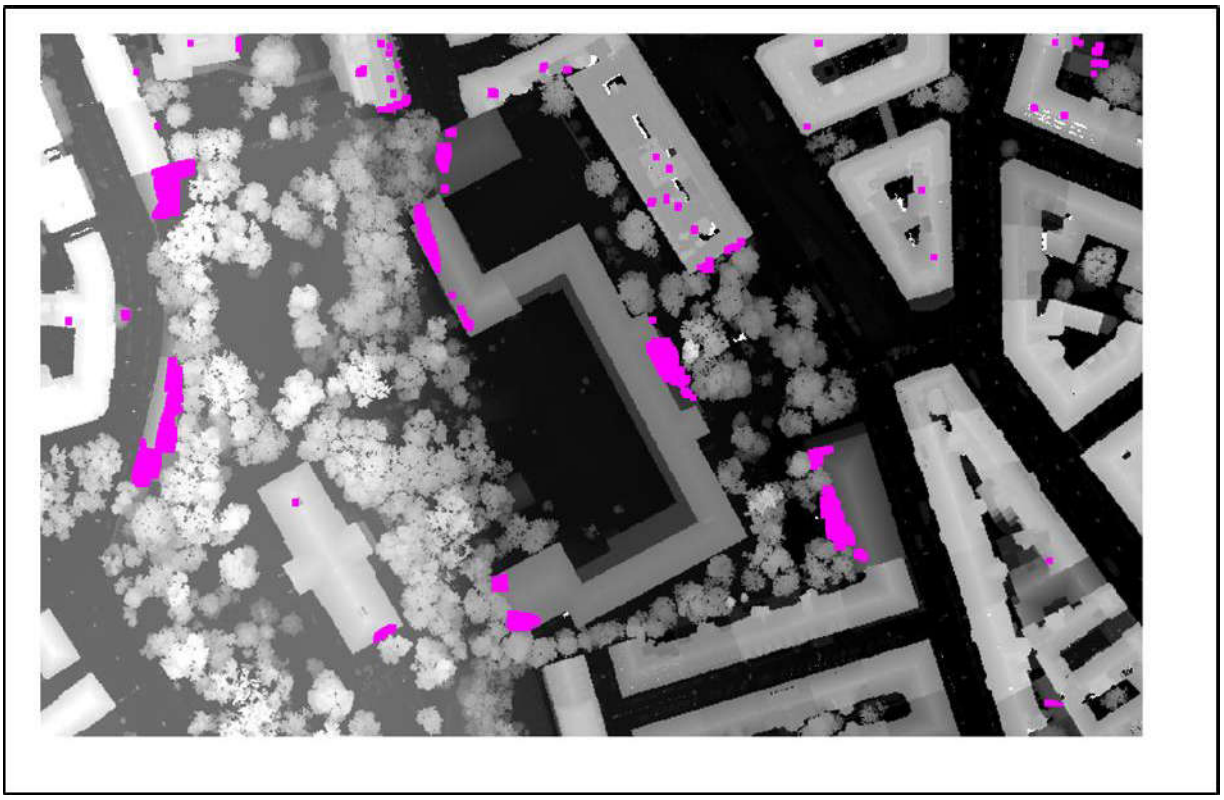

Figure 21: Solar irradiation difference map. Vegetation excluded minus vegetation included

5.2. Comparison of the Equinoxes

An equinox is an astronomical event that occurs twice a year around the 21st of March and the 23rd of September. For the year 2015 the March Equinox occurred on the 20th of March at 22:45 UT and the September Equinox on September 23rd at 8:21 UT. This event marks the moment, when the Sun is at zenith over the equator. Therefore the solar irradiation performance has to be the same for both equinoxes. To prove that, the solar irradiation maps for both days over the whole test area have to be compared with each other in every program. Figure 22 depicts a cross-correlation between the solar irradiation values at the spring and autumn equinox of the year 2015, assessed by ArcMap. A high level of correlation is observable in the visualization. A Histogram that shows the distribution of solar irradiation for both equinoxes is displayed in figure 23. The similarity of both results is observable.

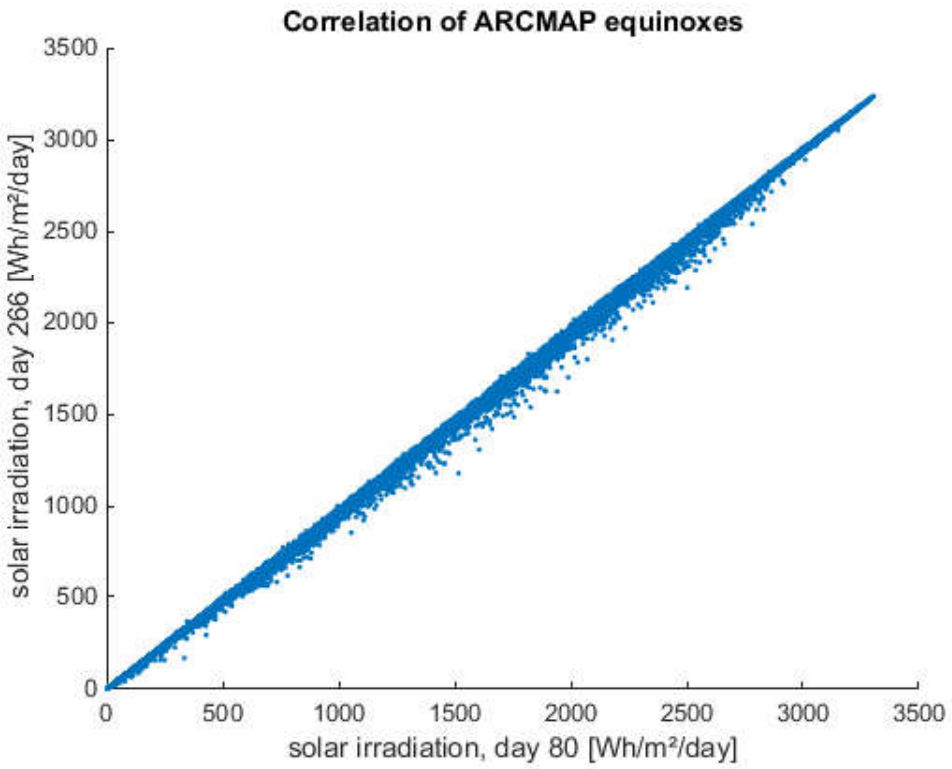

Figure 22: Comparison of the solar irradiation performance of the spring and autumn equinox of the year 2015

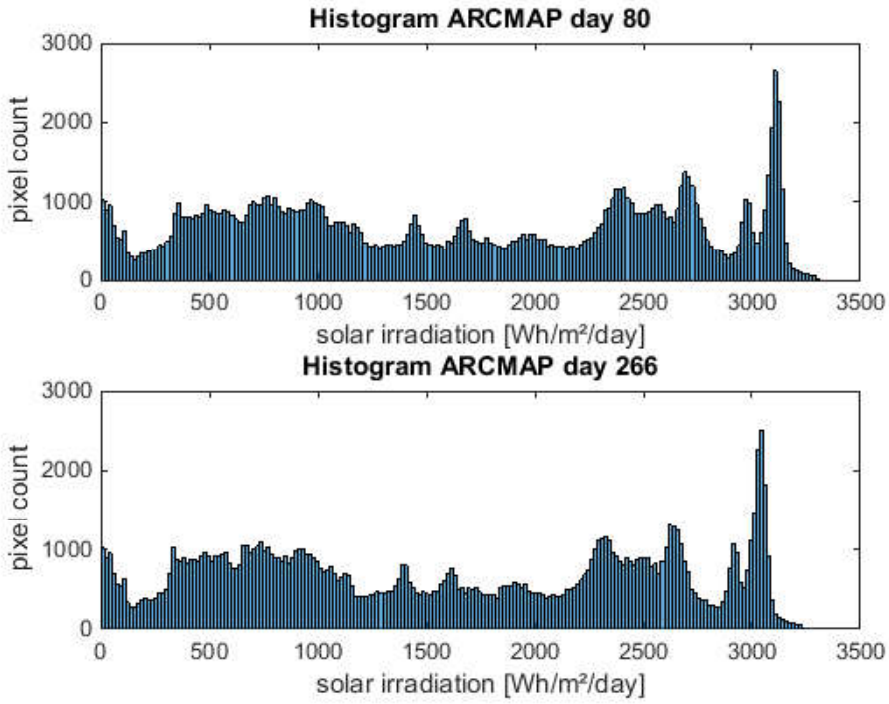

Figure 23: Distribution of solar irradiation values for both equinoxes

5.3. Solar irradiation comparison

As mentioned before, daily values of solar irradiation are calculated for a small subset of the test area, to simplify the comparison. Three special days were selected: The 21st of March (day 80), the 21st of June (day 172), and the 21st of December (day 355). On the 21st of March and on the 23rd of September respectively, the equator's plane passes the centre of the Sun. This astronomical event is called equinox. In respect to the Sun's position, the solar irradiation calculation for the day of an equinox has to yield similar results. A solstice also occurs twice a year as the Sun reaches its highest or lowest excursion relative to the celestial equator on the celestial sphere. It is either the longest or the shortest day of the year for all locations on the Earth, except for site which are located exactly on the equator, where day and night have the same durations over the whole year. The event of a solstice occurs around the 21st of June and the 21st of December each year. It is assumed that the solar irradiation is the strongest on the day of the summer solstice and the lowest on the day of the winter solstice, respectively.

The following table (table 12) shows statistical analysis results of global irradiation in the selected subset of the test area. Each pixel in the raster map represents global irradiation in

Wh/m²/day for the single days. All three programs use the same elevation model of the investigated area. The mean values for QGIS and VOSTOK are bigger than the values of ArcMap's Solar Analyst for all analysed days. Moreover the resulting maps of QGIS and VOSTOK show a broader bandwidth of irradiation values. Therefore their standard deviations are much higher than the ones for ArcMap. The map that is calculated with VOSTOK has a pixel size of 1 x 1 m². The size of each pixel in QGIS and ArcMap is 25 x 25 cm². The resulting maps of QGIS and VOSTOK have a high correlation. This becomes unequivocal by looking at all statistical measures.

Program	**ARCMAP**	**QGIS**	**VOSTOK**
Mean value [Wh/m²/day]			
Day 80 (2015.03.21.)	1,640	3,893	3,924
Day 172 (2015.06.21.)	3,854	6,658	6,551
Day 355 (2015.12.21.)	199	1,333	1,370
Maximum [Wh/m²/day]			
Day 80 (2015.03.21.)	3,311	7,547	7,322
Day 172 (2015.06.21.)	5,775	9,730	8,908
Day 355 (2015.12.21.)	648	4,777	4,499
Minimum [Wh/m²/day]			
Day 80 (2015.03.21.)	0.1	432	334
Day 172 (2015.06.21.)	0.2	599	626
Day 355 (2015.12.21.)	0.2	197	152
Standard deviation [Wh/m²/day]			
Day 80 (2015.03.21.)	963	2,129	1,954
Day 172 (2015.06.21.)	1,432	1,960	1,935
Day 355 (2015.12.21.)	169	1,242	1,096

Table 12: Statistical measures of the solar irradiation maps of all programs

The above mentioned discrepancies between the mean values of the results for the same days, which are obtained by means of different programs, are higher than expected. The programs apply different approaches which use distinct input parameters to perform the calculation of the daily solar irradiation. Since all three programs calculate solar irradiation values for each pixel of the same surface model and the same days, the parameters which describe the

atmosphere and the surface are supposed to be the reason for the divergent results (see chapter 4.4).

Figure 24 depicts histograms, retrieved from all irradiation maps for the day 80 of the year 2015. It represents the distribution of solar irradiation values in the selected test area.

The distribution of the values in the map that is assessed with ArcMap has a rather narrow bandwidth, compared to the maps of the other two programs. One significant peak in the region of high solar irradiation values (3200 Wh/m²/day) is noticeable in its histogram. There is a minimum close to the peak at values around 2800 Wh/m²/day. The rest of the values are almost equally distributed without any noticeable maxima or minima.

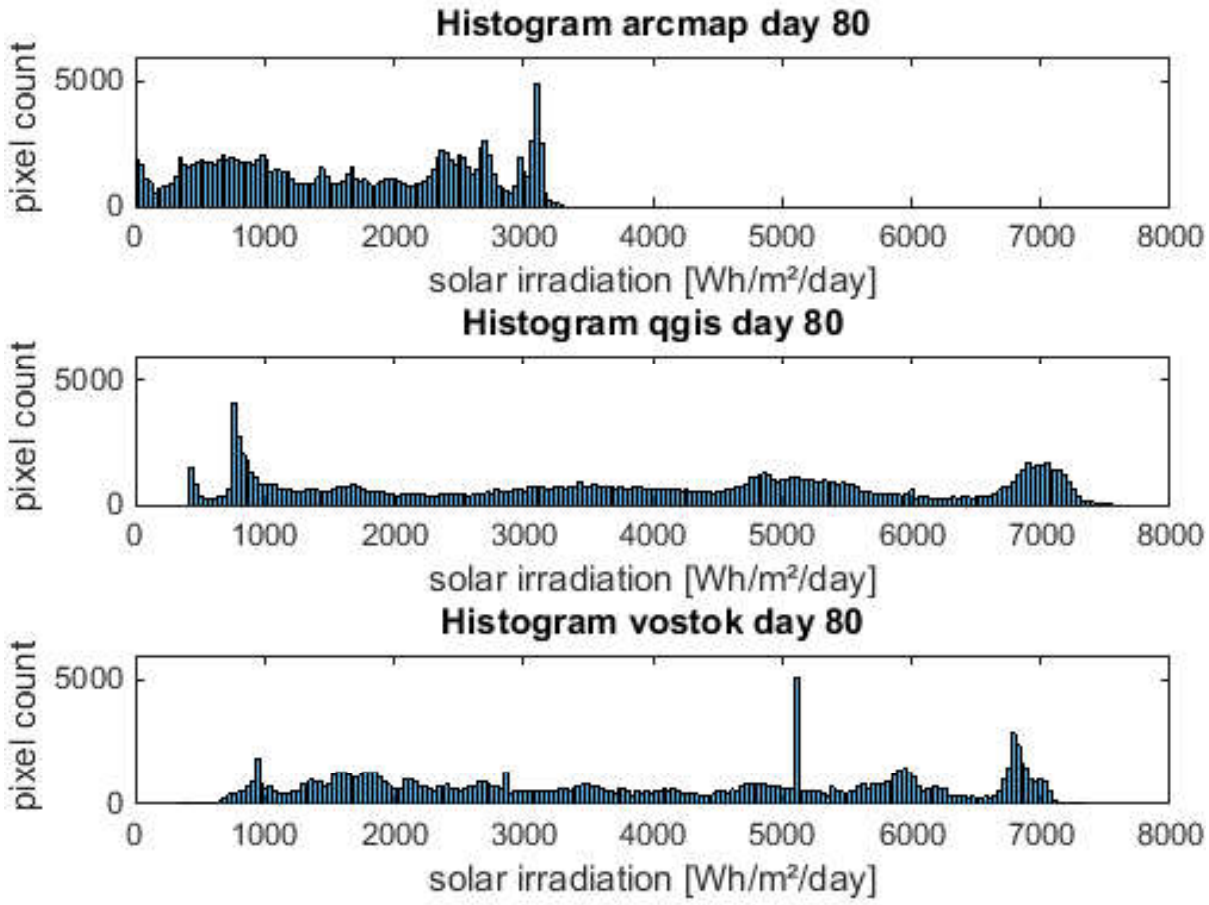

Figure 24: Histogram of global irradiation values for the 21st of March obtained with ArcMap's solar analysis tool, QGIS r.sun and VOSTOK

The solar radiation maps of QGIS and VOSTOK contain a higher diversity of values than the comparable map of ArcMap. The histograms of the solar irradiation map obtained with QGIS

and VOSTOK display one maximum at low and one at high values, whereas VOSTOK has an additional high, but narrow peak at solar irradiation values around 5200 Wh/m²/day. The explanation for this phenomenon is the large pixel size (1 x 1 m²) of the solar irradiation map of VOSTOK. It is 16 times bigger than the pixel size of the comparable maps in ArcMap and QGIS (25 x 25 m²) and represents the mean of the 16 values. In an advanced processing step the pixel size of all maps is set equal, to enable a statistical comparison in Matlab. However, the VOSTOK map does not generate new values for the increased number of pixels. Thus the same value (mean value) is allocated to a group of 16 pixels and the number of pixels which represent the same values is increasing, because the new value is the statistical mean of the 16 single pixels. For the visualization of the solar irradiation map in a histogram similar pixels are combined in a group due to their solar irradiation value. Every bar in the histogram represents one group of similar solar irradiation values with a lower and upper threshold, which are generated automatically by Matlab.

About 300,000 pixels are classified as roof areas in the analysed subarea. To correlate the datasets and yield a reasonable visualization in a scatter plot, a smaller sample of 50,000 values is selected randomly. Figure 25 shows a cross-correlation of solar irradiation values obtained with ArcMap and QGIS processing for the 21st of March. In other words, the solar irradiation maps are compared with each other in a pixel-wise manner for the three specific days of the year 2015. Therefore it is not possible to involve the result of VOSTOK in this analysing step, due to its different pixel size. Figure 26 and 27 depict the remaining possible comparisons (21st of July and 21st of December). It is noticeable that there are no small values close to zero for the solar irradiation calculation with QGIS. A pattern, where most of the points in the graph are spread out from the bottom left corner to the top right corner, is visible for March 21st (day 80) and December 21st (day 355). The similarity of the two results for June 21st is insignificant. Therefore the correlation is higher for the sample of solar irradiation values for the day 80 and 355 than for the day 172.

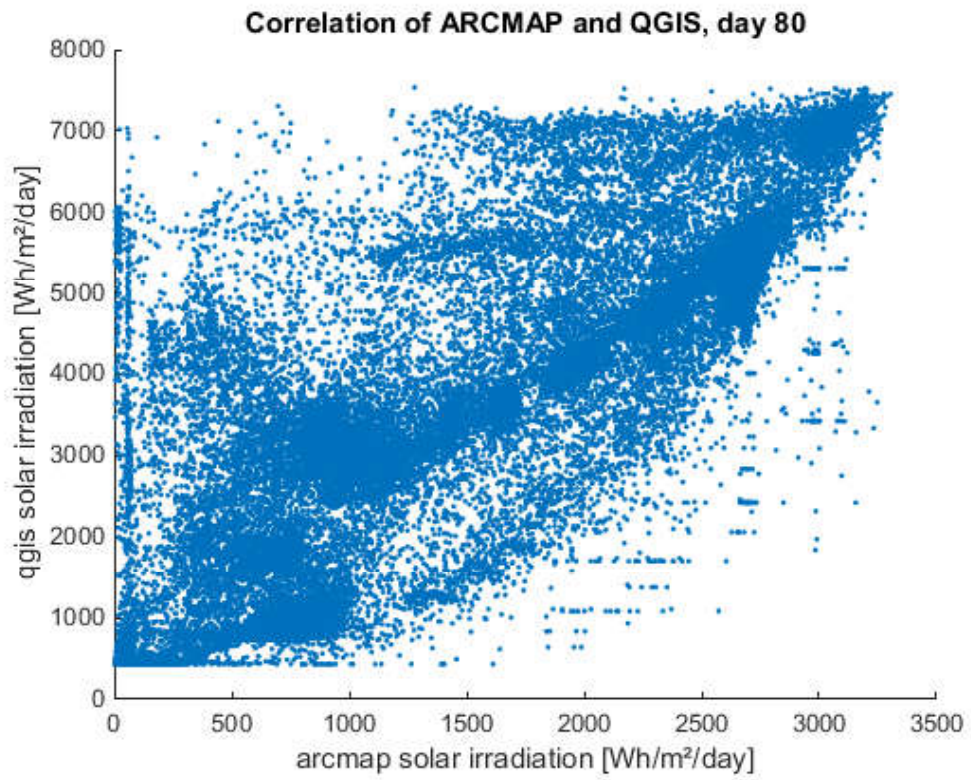

Figure 25: Relative comparison of QGIS and ArcMap solar irradiation map for the 21st of March through a cross-correlation. A sample of 50,000 pixels was selected randomly.

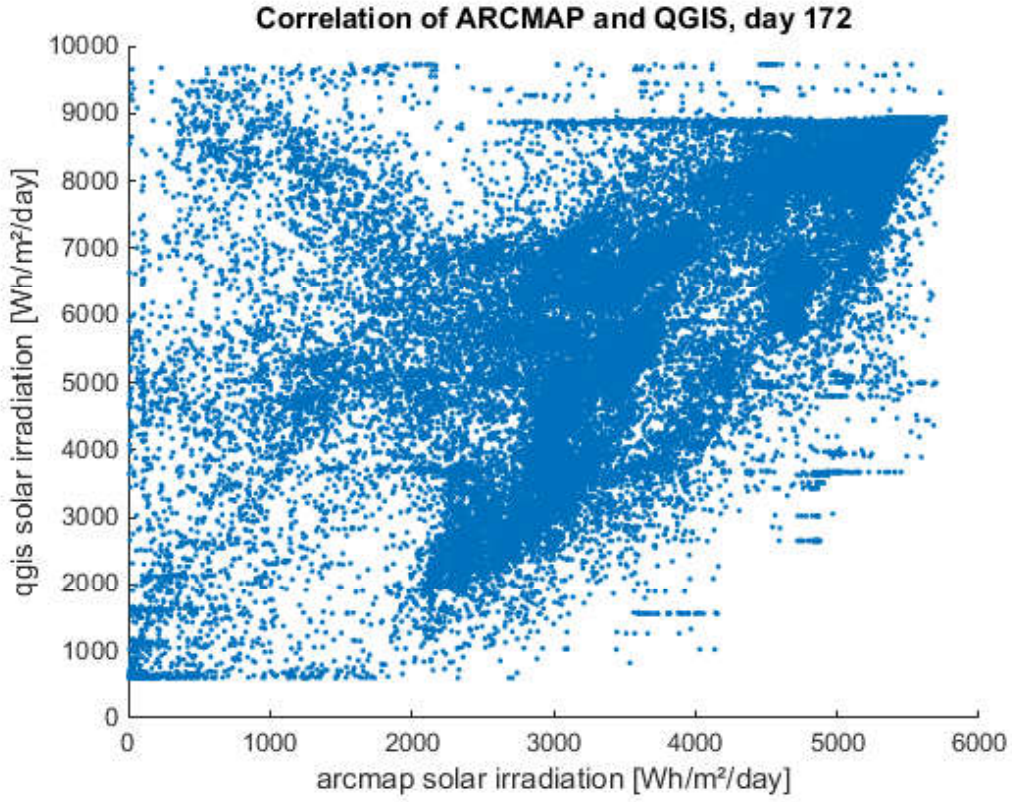

Figure 2: Relative comparison of QGIS and ArcMap solar irradiation map for the 21st of June through a cross-correlation. A sample of 50,000 pixels was selected randomly.

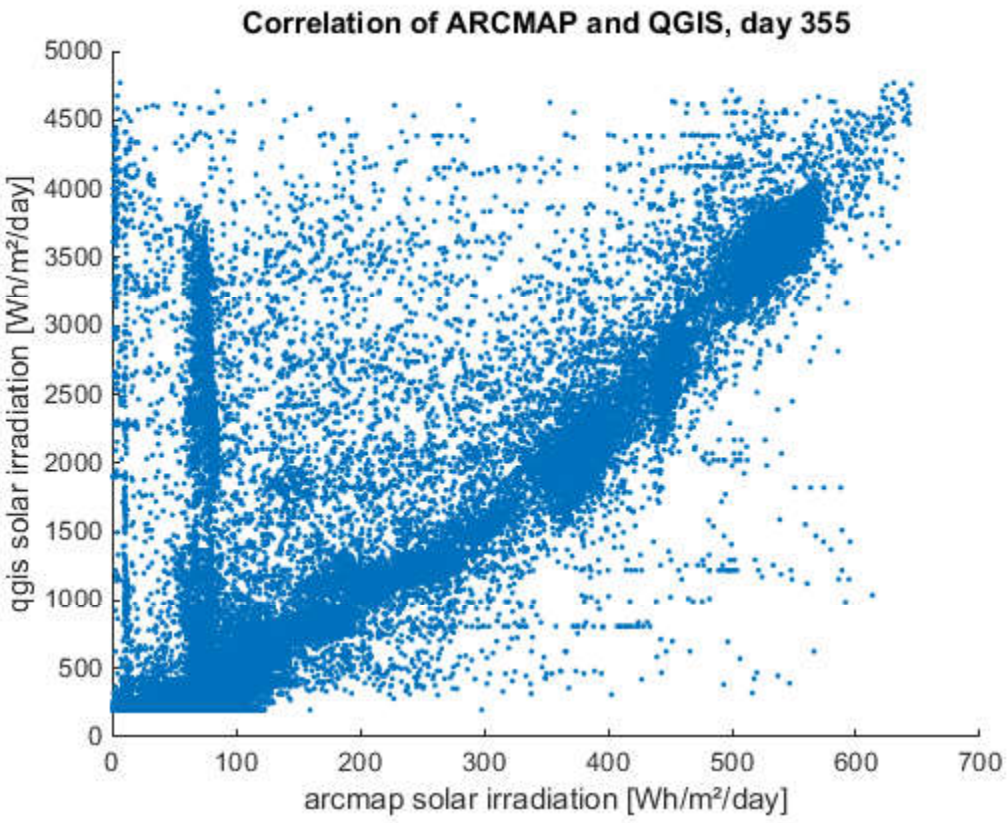

Figure 27: Relative comparison of QGIS and ArcMap solar irradiation map for the 21st of December through a cross-correlation. A sample of 50,000 pixels was selected randomly.

5.4. Deactivation of the atmospheric influence

The high differences between the solar irradiation values assessed with ArcMap and the results of QGIS and VOSTOK necessitate further analysis. Atmospheric and surface parameters are the only inputs that differ in the programs. The solar potential calculation with VOSTOK is not capable to influence these input variables, nor can they even be seen by the user. As mentioned already, it is still in the development stage. Nevertheless is can be assumed that VOSTOK uses a similar algorithm to QGIS, due to the small deviation for all statistical values of the individual solar irradiation maps. Only ArcMap and QGIS are considered in this chapter.

In the first step the default values for the parameters are changed to values which neglect the atmospheric influence and the surface reflection on the total radiation. Then the solar irradiation is calculated - like before - in a pixel-wise manner. After that the raster maps, which represent the solar irradiation distribution of the test area, are compared with each other. Table 13 outlines statistical parameters of the irradiation maps for the 21st of March

processed by ArcMap and QGIS to analyse the atmospheric and ground reflecting influences. The differences for all parameters decrease after neglecting the atmosphere and the surface parameter in the computation of solar irradiation performance.

Day 80	**Atmospheric effects and surface reflection included**	**Atmospheric effects and surface reflection excluded**
ArcMap mean	1,640	5,225
QGIS mean	3,893	4,792
Difference	**2,253**	**433**
ArcMap minimum	0	0
QGIS minimum	432	1
Difference	**432**	**1**
ArcMap maximum	3,311	10,443
QGIS maximum	7,547	9,064
Difference	**4,236**	**1,379**
ArcMap standard deviation	963	2,901
QGIS standard deviation	2,129	2,553
Difference	**1,166**	**348**

Table 13: Statistical Parameters of 4 different solar irradiation maps on March 21st – Arcmap with atmosphere and surface refection, Arcmap without atmosphere and surface reflection; the same for QGIS

Figure 28 is a visualization of the distribution of solar irradiation values in two resulting maps. The atmospheric effects and the ground refection are not involved in the calculation procedure. It is noticeable that ArcMap's solar irradiation map has a high amount of pixels that represent a very low value. QGIS's map shows two significant peaks at values around 6000 Wh/m²/day and 6600 Wh/m²/day respectively.

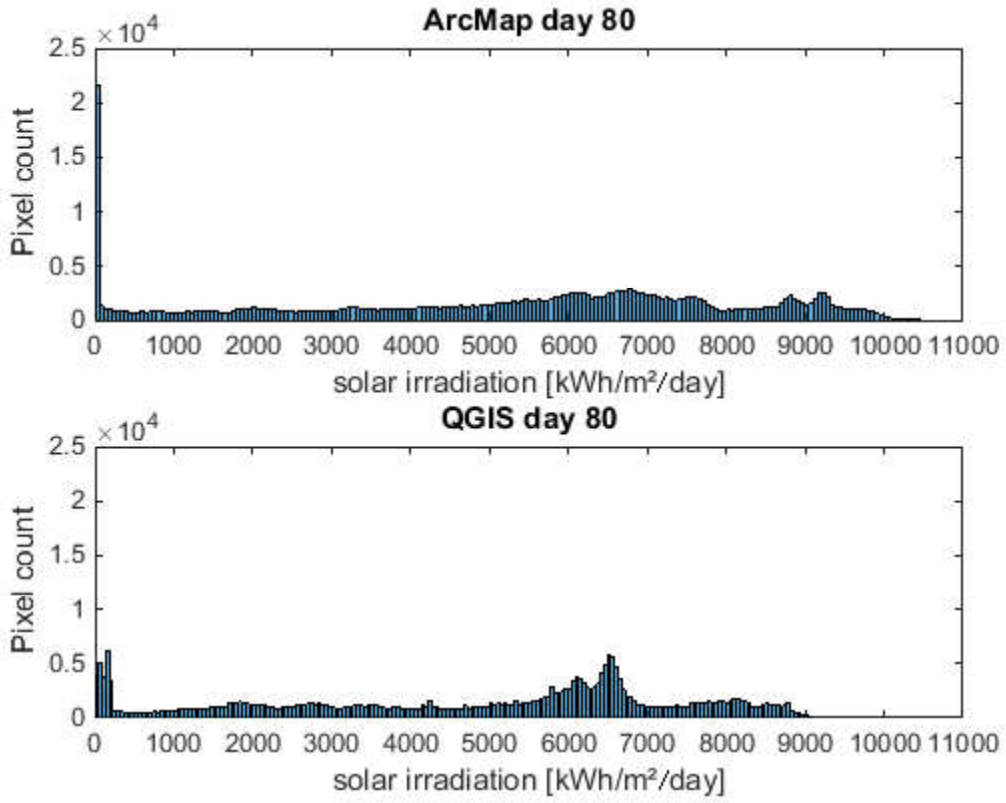

Figure 28: Histograms of the solar irradiation maps without atmospheric effects and surface reflection on the irradiation performance

6. DISCUSSION

The hypothesis that was stated in chapter 1.3 is checked and discussed in this section by making references to the obtained results.

The influence of objects outside the roof areas on the solar irradiation performance on rooftops was significant for the observed test area over the whole year. The comparison of a solar irradiation assessment, where these objects were included as potential shadow causer, with a calculation methodology, where only man-made objects were considered as obstacles for the Sun rays reveals that there is a distinct discrepancy between these two approaches. In particular in areas with a high amount of vegetation with short distances to buildings the influence of objects outside of roof areas is high. The difference between the mean values of the two solar irradiation maps is 1582 kWh/m²/Day and is considered significant. The mean values in the map that includes all objects is 734,757 kWh/m²/year and 736,339 kWh/m²/year for the map without any other objects than roof areas. This finding leads to the use of an elevation model that contains objects of the surface (DSM). The DSM has a resolution of 625 cm². The test area in Vienna requires the integration of pixels that are located outside of the rooftops for the computation of a solar irradiation map.

VOSTOK's estimation of solar irradiation yields values of a smaller expansion than the original test area. A subset of the test area, where all three programs output values was chosen to perform a proper comparison. Furthermore, the resulting resolution is 1 m². ArcMap and QGIS yield an output resolution that is identical to the DSM's resolution (625 cm²).

The hypothesis that the single resulting solar irradiation raster maps which are assessed by different programs based on the same DSM output similar distributions of irradiation values is only partly true. The results are discussed in the following paragraphs.

ArcMap's Solar Analyst and QGIS's r.sun tool include different atmospheric parameters and algorithms in their calculations, whereas VOSTOK does not provide any information about parameters or the applied algorithm.

ArcMap uses two parameters that describe the weakening influence of the atmospheric condition on the incoming solar radiation. They are defined as **atmospheric parameters** and are called **Transmittivity** and **Diffuse Proportion**. ArcMap's Solar Analyst only considers the direct and diffuse component of the radiation in its calculation algorithm to obtain global irradiation values. QGIS offers only one parameter that refers to the atmospheric influence. It

is called **Linke atmospheric turbidity**. The algorithm that is implemented in the solar irradiation assessment of QGIS's r.sun tool also incorporates, in addition to the direct and diffuse, the ground reflected component of the solar radiation. **Albedo** is the quantity that describes the additional reflected component and is defined as a **topographic parameter**.

By using the default values for the atmospheric and topographic parameters, which are editable in the programs ArcMap and QGIS, the outputs for single days differ greatly. The smallest difference in solar irradiation mean values is 1134 Wh/m²/day for the 21st of December. QGIS and VOSTOK show a higher correlation, although VOSTOK has a coarser resolution in the resulting map, as mentioned above. The difference in the mean values of solar irradiation lies between 31 Wh/m²/day for March 21st and 107 Wh/m²/day for the 21st of June. It can be assumed that VOSTOK and QGIS work with a similar algorithm and atmospheric and topographic parameters.

High correlating results for ArcMap and QGIS could only be obtained by modifying the input parameters as follows: Firstly, the atmospheric parameters must be deactivated so that the atmosphere has no influence on the incoming solar irradiance at all. Secondly the albedo parameter, that is a part of the QGIS input architecture, must be set to zero. Hence the ground reflected component is not considered in the calculation of the solar irradiation potential in QGIS. This was necessary, in order to obtain similar results for both programs. ArcMap neglects this component as well. The difference between the mean value of solar irradiation assessed by ArcMap and QGIS for March 21st of 2015 accounts only for 433 Wh/m²/day when the editable parameters are changed as described above. Other analyzed days yield similar discrepancies. The implementation of a solar irradiation estimation for the same day with default input parameters gives a difference of 2,253 Wh/m²/day for the mean values.

7. CONCLUSION

A GIS-based method to estimate the solar performance of an area is applied in this study. The test area is located in an urban neighborhood with mainly residential character. Big buildings with pitched roofs that are connected to each other characterized the structure of this area. The terrain is mostly flat and homogenous. Furthermore mostly randomly oriented streets and scattered small parks are present in the environment. The vegetation causes shadows on some rooftops that in turn influence the solar irradiation on these locations. Even though the vegetation has a minor propagation, its impact on solar irradiation values is significant throughout the year and cannot be neglected. Therefore a Digital Surface Model (DSM), that includes the vegetation, must be used as a base of the estimation of solar potential by using a GIS-based method. It can be assumed that this is the case for whole Vienna and cities that are comparable in respect to their architectural and topographical characteristics. It must be mentioned here that the seasonal change in the vegetation is not considered in the analysis at all.

In order to reduce computational costs only daily values of solar irradiation are calculated in a pixel-wise manner. Four special days are selected throughout the year 2015: The two equinoxes (March 21st and September 23rd) and the two solstices (June 21st and December 21st). As expected, the highest daily values of solar irradiation per square meter are obtained on the 21st of June and the lowest at the 21st of December in all programs. The results for the 21st of March and the 23rd of September yield highly correlated irradiation maps, due to the similarity in the positions of the Sun towards the Earth on the two days.

The utilization of default values for the editable parameters in ArcMap and QGIS reveal high discrepancies for all observed days between the two programs. QGIS and VOSTOK yield similar results. After ignoring the atmospheric influence in ArcMap and QGIS and the ground reflected component in QGIS, the results of the two programs are highly correlated. Hence they implement distinct algorithms to solve the problem of solar irradiation assessment over an area of interest. Unfortunately, VOSTOK lacks information about included parameters and used algorithm. It can only be assumed that the algorithm and the parameters are similar to the default adjustments of QGIS, due to the findings of this study.

The limitations of the comparison of the three programs cannot be neglected. First of all, VOSTOK offers no insight to the used algorithm or variables that influence the solar radiation. It is only an assumption that they are similar to QGIS because of their highly

correlated results for all observed days. The implemented algorithms and included parameters of QGIS and ArcMap are described in the manuals of the individual programs, both of which differ significantly. Thus a comparison of the results is only partly possible - by editing the input parameters as described in chapter 6.

In general, the individual solar irradiation assessment programs use different algorithms and parameters to describe the impact of solar radiation on an arbitrary surface on the Earth. The influence of the vegetation has to be considered in the calculation process, even though its distribution is minor in the analyzed urban area. The state of the atmosphere also has a significant impact on the solar irradiation performance.

References

Angles J., Ménard L., Bauer O., Rigollier Ch., Wald L., 1999. A climatological database of the Linke turbidity factor. ISES Solar World Congress 1999, July 1999, Jerusalem, Israel. ISES, 1, pp. 432-434

Assmann D., Laumanns U., Uh D., 2006. Renewable Energy – A Global Review of Technologies, Policies and Markets. Earthscan, London, UK

Axelsson, P., 2000. DEM generation from laser scanner data using adaptive TIN models. *International Archives of the Photogrammetry and Remote Sensing*, Vol. XXXIII Part B4/1, pp. 110-117

Bechtold S., 2015. VOSTOK: Voxel Octree Solar Toolkit. LiDAR Research Group, Abteilung für Geoinformatik, Universität Heidelberg. URL: http://www.uni-heidelberg.de/lrg.

Besharat F., Dehghan A., Faghih A., 2013. Empirical Models for estimating global solar radiation: A review and case study. *Renewable and Sustainable Energy Reviews,* 21, pp. 798-821

Chaves A; Bahill T., 2010. Locating Sites for Photovoltaic Solar Panels. *ArcUser, the Magazine for ESRI Software User*, Fall 2010, Vol.13/4, pp 24-27

Chen C. J., 2011. Physics of Solar Energy. Wiley, UK

Compagnon, R., 2004. Solar and Daylight Availability in the Urban Fabric. *Energy and Buildings*, Vol. 36/4, pp 321-328

Cros S.; Wald L., 2003. Survey of the main databases providing solar radiation data at ground level. Rudi Goossens. 23rd EARSeL Annual Symposium "Remote Sensing in Transition", Jun 2003, Ghent, Belgium. Milpress, pp.491-497

Eurostat, 2015.
http://ec.europa.eu/eurostat/statistics-explained/index.php/Renewable_energy_statistics/de
Renewable Energy Statistics, Eurostat

Fink Ch., Müller T., Weiss W., 2009. Solarwärme 2020 – Eine Technologie- und Umsetzungsroadmap für Österreich. Arbeitsgemeinschaft Erneuerbare Energie INTEC, Vienna, Austria

Freris L., Infield D., 2008. Renewable Energy in Power Systems. Wiley, UK

Fu P., Rich P., 1999. Design and Implementation of the Solar Analyst: an ArcView Extension for Modeling Solar Radiation at Landscape Scales. Proceedings of the Nineteenth Annual ESRI User Conference

Hofierka J., Suri M., 2007. http://grass.osgeo.org/grass64/manuals/r.sun.html. GeoModel s. r. o., Bratislava, Slovakia

Hofierka J., Kanuk J., 2009. Assessment of Photovoltaic Potential in Urban Areas Using Open-Source Radiation To
ols. *Renewable Energy* (34); pp 2206–2214

Hofierka J., Suri M., 2002. The solar radiation model for Open source GIS: implementation and applications. *Proceedings of the Open source GIS – GRASS users conference 2002,* Trento, Italy

Hollaus M., 2006. Large Scale Applications of Airborne Laser Scanning for a Complex Mountainous Environment. Dissertation, Institut für Photogrammertrie und Fernerkundung, Technische Universität Wien

Höfle B., Mücke W., Dutter M., Rutzinger M., Dorninger P., 2009. Detection of Building Regions Using Airborne LIDAR – a New Combination of Raster and Point Cloud Based GIS Methods. *Proceedings of the AGIT Symposium 2009,* Salzburg, Austria

IPCC, 2014: Summary for policymakers. In: Climate Change 2014: Impacts, Adaptation, and Vulnerability. Part A: Global and Sectoral Aspects. Contribution of Working Group II to the Fifth Assessment Report of the Intergovernmental Panel on Climate Change [Field, C.B., V.R. Barros, D.J. Dokken, K.J. Mach, M.D. Mastrandrea, T.E. Bilir, M. Chatterjee, K.L. Ebi, Y.O. Estrada, R.C. Genova, B. Girma, E.S. Kissel, A.N. Levy, S. MacCracken, P.R. Mastrandrea, and L.L.White (eds.)]. Cambridge University Press, Cambridge, United Kingdom and New York, NY, USA, pp. 1-32

Jochem A., Höfle B., Rutzinger M., Pfeifer N., 2009. Automatic Roof Plane Detection and Analysis in Airborne Lidar Point Clouds for Solar Potential Assessment. *Sensors 2009,* 9(7), pp. 5241-5262

Jochem A., Höfle B., Rutzinger M., 2011. Extraction of Vertical Walls from Mobile Laser Scanning Data for Solar Potential Assessment. *Remote Sensing 2011,* 3, pp. 650-667

Kalogirou S., 2009. Solar Energy Engineering – Processes and Systems. Elsevier, USA

Kraus, K., Pfeifer, N., 1998. Derivation of digital terrain models in wooded areas with airborne laser data. *ISPRS Journal of Photogrammetry and Remote Sensing*, 53(4), pp. 193-203

Linke F., 1922. Transmissionskoeffizient und Trübungsfaktor. *Beiträge zur Physik der freien Atmosphäre,* 10, pp. 91-103

Marion B., Anderberg M., George R., Gray-Hann P., Heimiller D., 2001. PVWATTS Version 2 – Enhanced Spatial Resolution for Calculating Grid-Connected PV Performance. *Conference Paper for the NCPV Program Review Meeting* in Lakewood, CO, 14-17 Oct 2001, National Renewable Energy Laboratory, Golden. CO, USA

Melius J.; Margolis R.; Ong S., 2013. Estimating Rooftop Suitability for PV: A Review of Methods, Patents, and Validation Techniques. Technical Report NREL/TP-6A20-60593. Dec 2013, National Renewable Energy Laboratory, Golden, CO, USA

Myers D., 2013. Solar Radiation. CRC Press, Boca Raton, Florida, USA

Navigant Consulting, Inc. 2007. California Rooftop Photovoltaic (PV) Resource Assessment and Growth Potential by County. California Energy Commission, PIER (Public Interest Energy Reserach) Program, San Francisco, CA, USA

Page J.K., 1986. Prediction of solar radiation on inclined surfaces. *Solar Energy R&D in the European Community, Series F: Solar radiation data,* Vol. 3, D. Reidel Publishing Company, Dordrecht

Paulescu M.; Paulescu E.; Gravila P.; Badescu V., 2013. Weather Modeling and Forecasting of PV Systems Operation. *Green Energy and Technology,* London, Springer, pp. 17-42

Perez R., Ineichen P., Moore K., Kmiecik M., Chain C., George R., Vignola F., 2002. A new operational Satellite-to-Irradiance Model – Description and Validation. *Manuscript Submitted to Solar Energy 4/2002*

Perez-Garzia J. L., Delgado J., Cardenal J., Colomo C., Urena M. A., 2012. Progressive Densification and Region Growing Methods for Lidar Data Classification. *International Archives of the Photogrammtery , Remote Sensing and Spatial Information Science,* Vol. XXXXIX-B3, XXII ISPRS Congress, 25. Aug – 01 Sept. 2012, Melbourne, Australia

Pfeifer N., Stadler P., Briese C., 2001. Derivation of digital terrain models in the SCOP++ environment. *Proceedings OEEPE Workshop on Airborne Laserscanning and Interferometic SAR for Digital Elevation Models*, Stockholm, 2001, pp. 1-13

Pfeifer N., Mandlburger G., Otepka J., Karel W., 2014. OPALS – A framework for Airborne Laser Scanning data analysis. *Computers, Environment and Urban Systems,* Vol. 45, pp. 125 - 136

Rich P., 1989. A Manual for Analysis of Hemispherical Canopy Photography. Los Alamos National Laboratory, Department of Biological Science, Stanford University, Stanford, USA

Spellman F., Bieber R., 2011. The Science of Renewable Energy. CRC Press, USA

Suri M., Huld T., Dunlop E., Ossenbrink H., 2007. Potential of solar electricity generation in the European Union member states and candidate countries. *Solar Energy 81*, pp 1295-1305

Suri M., Hofierka J., 2004. A newGIS-based solar radiation model and its application to photovoltaic assessments. *Transaction in GIS 8*, pp. 175-190

Tooke, T.R.; Coops, N.C.; Voogt, J.A.; Meitner, M.J., 2011. Tree Structure Influences on Rooftop-received Solar Radiation. *Landscape and Urban Planning* (102); pp. 73–81

Vardimon, R., 2011. Assessment of the Potential for Distributed Photovoltaic Electricity Production in Israel. *Renewable Energy* (36); pp. 591–594

Vignola F., Harlan P., Perez R., Kmiecik M., 2007. Analysis of satellite derived beam and global solar radiation data. *Solar Energy 81,* pp. 786-772

Vosselman, G. 2000. Slope based filtering of laser altimetry data. International *Archives of Photogrammetry and Remote Sensing*, XXXIII, Part B3, pp. 935-942

Wittmann, H.; Bajons, P., 1997. Identification of Roof Areas Suited for Solar Energy Conversion Systems. *Renewable Energy* (11:1); pp. 25–36

Wong, L. T.; Chow W. K., 2001. Solar radiation model. *Applied Energy 69 (2001),* pp. 191-224

Yu B., Liu H., Wu J., Hu Y., Zhang L., 2010. Automated derivation of urban building density using airborne LIDAR data an object-based method. *Landscape and Urban Planning* 98 (2010), pp. 210-219

Zelenka A., Perez R., Seals R., Renné D., 1999. Effective Accuracy of Satellite-Derived Hourly Irradiances. *Theoretical and Applied Climatology* 62, 199-207; Springer Verlag, Austria

Solar and PV data, 2015. http://solargis.info/doc/solar-and-pv-data. GeoModel Solar s. r. o., Bratislava, Slovakia

Appendix

The following figures depict visualizations of different solar irradiation maps, estimated by ArcMap's Solar Analyst tool with default values for all atmospheric parameters. The first three maps represent daily estimations of the solar irradiation. The last two maps show annual sums of solar irradiation with and without the influence of the vegetation. The irradiation values are classified in 7 groups in every map.

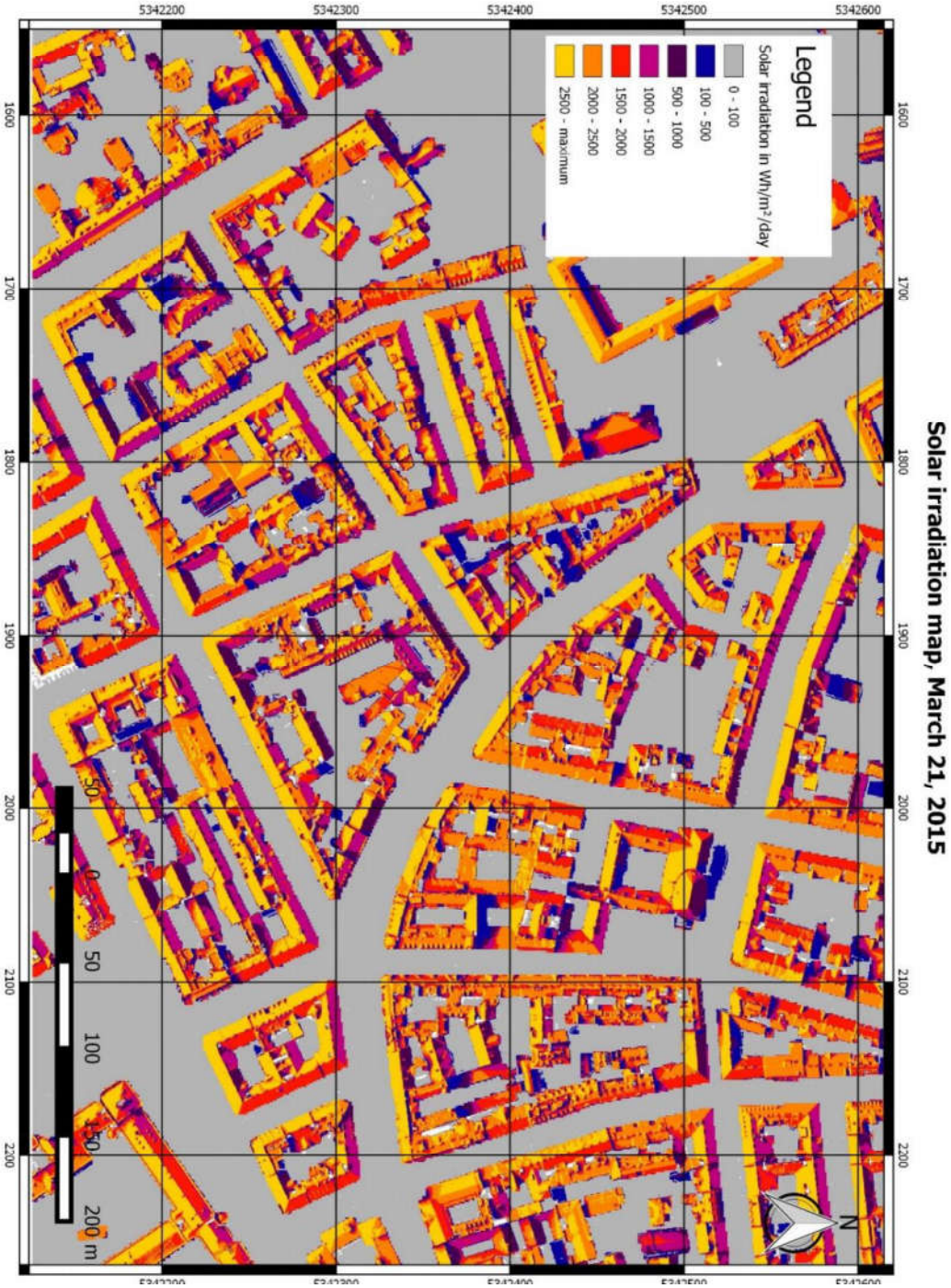

Solar irradiation map, July 21, 2015

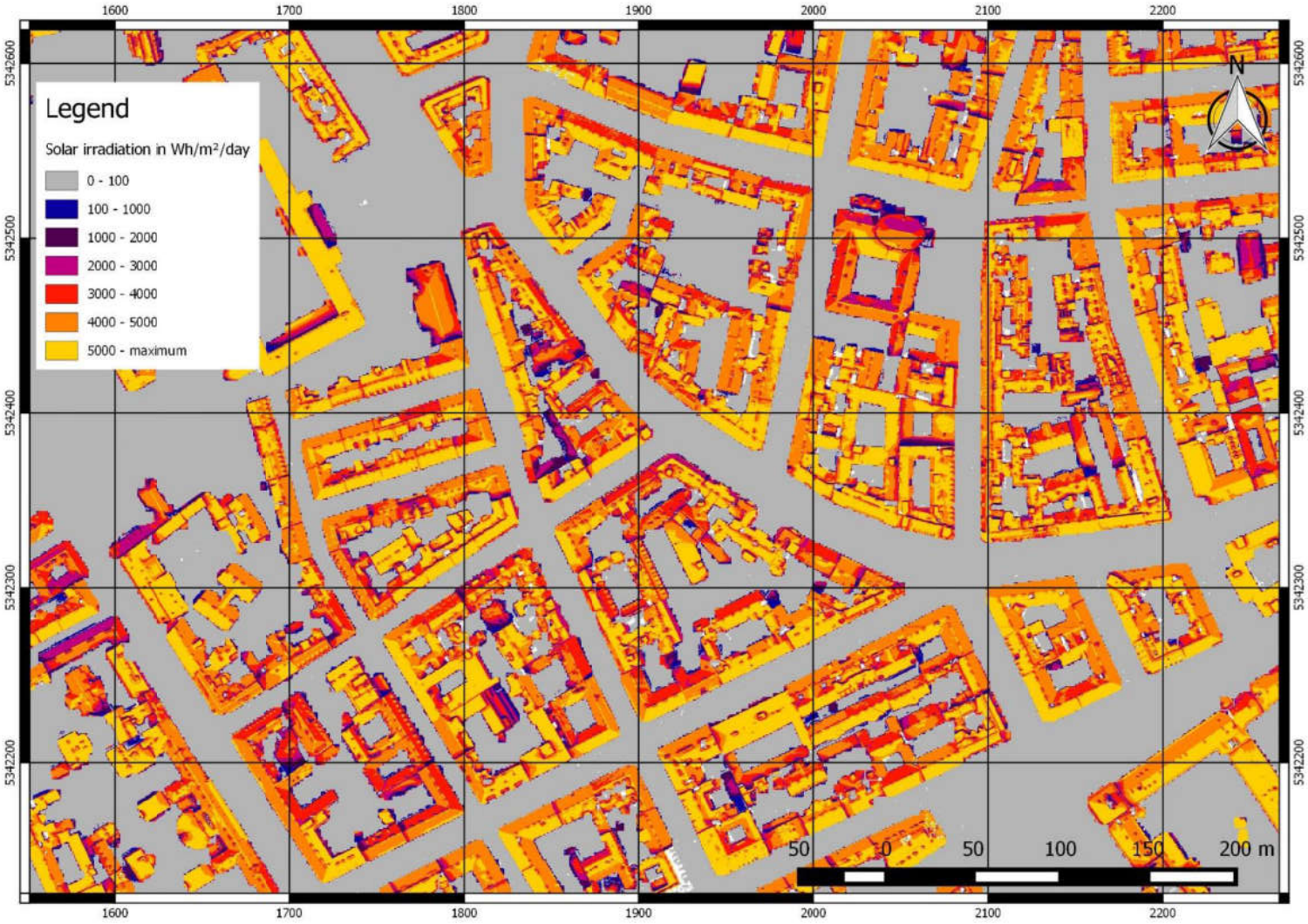

Solar irradiation map, December 21, 2015

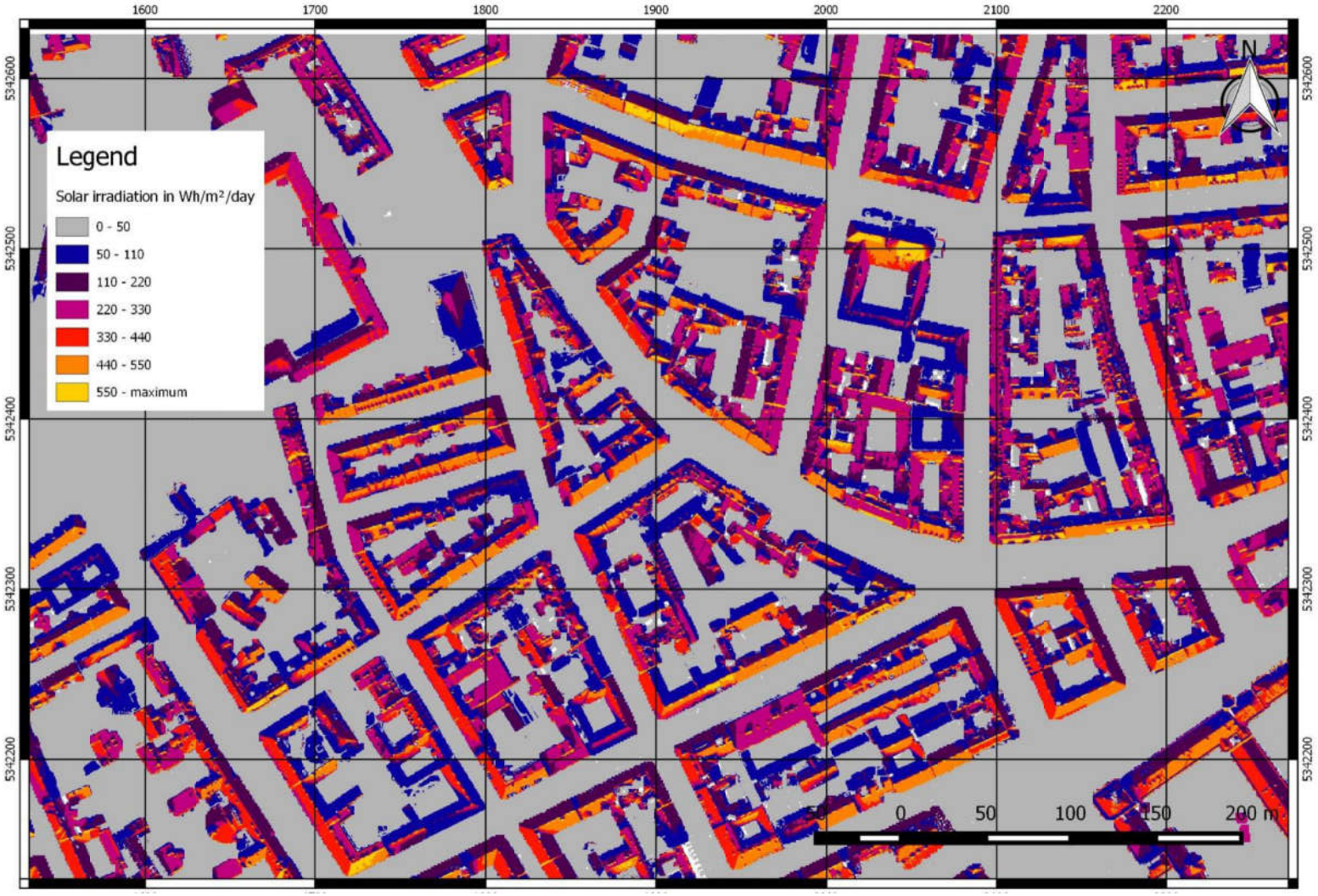

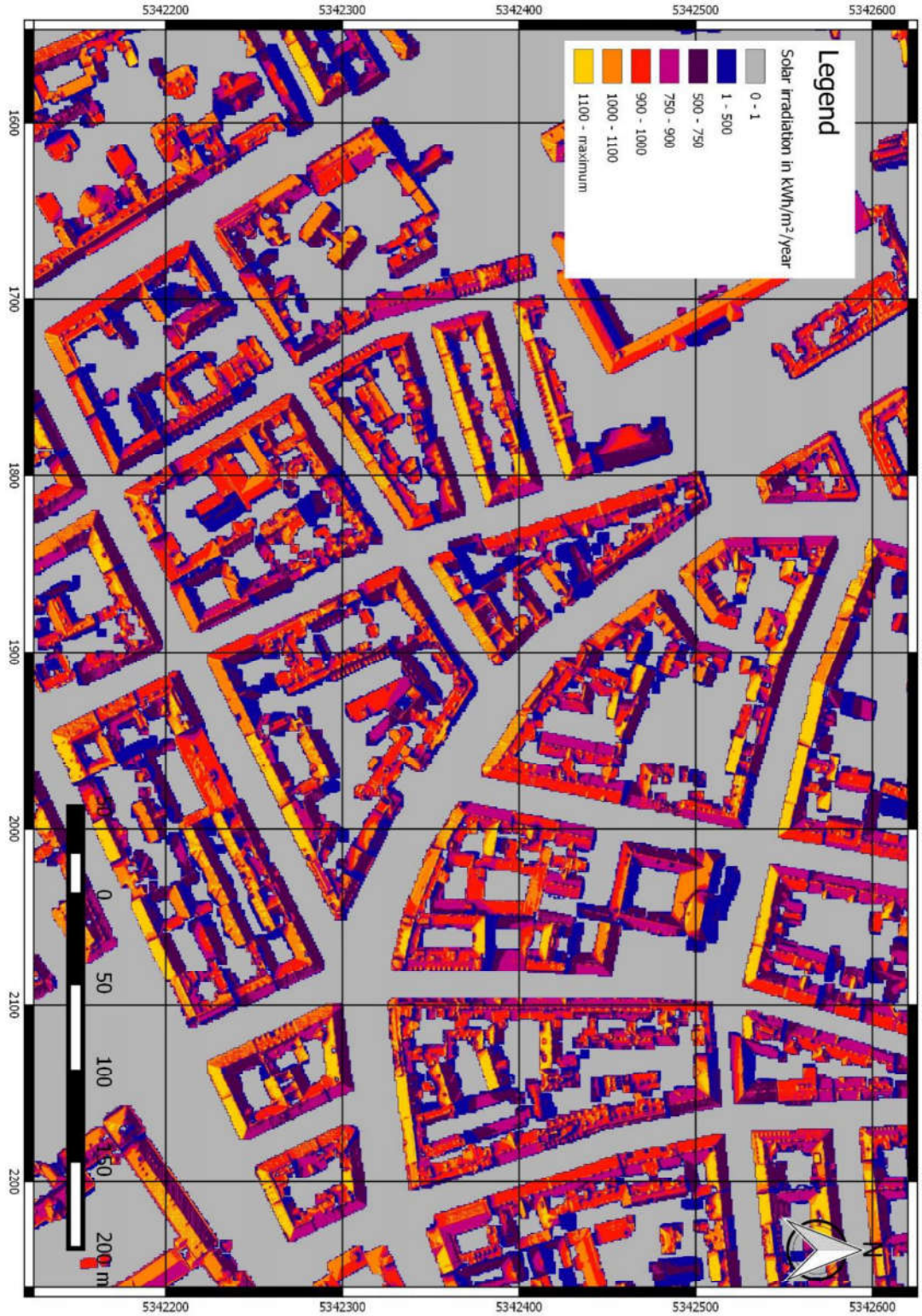

Solar irradiation map of 2015, vegetation included
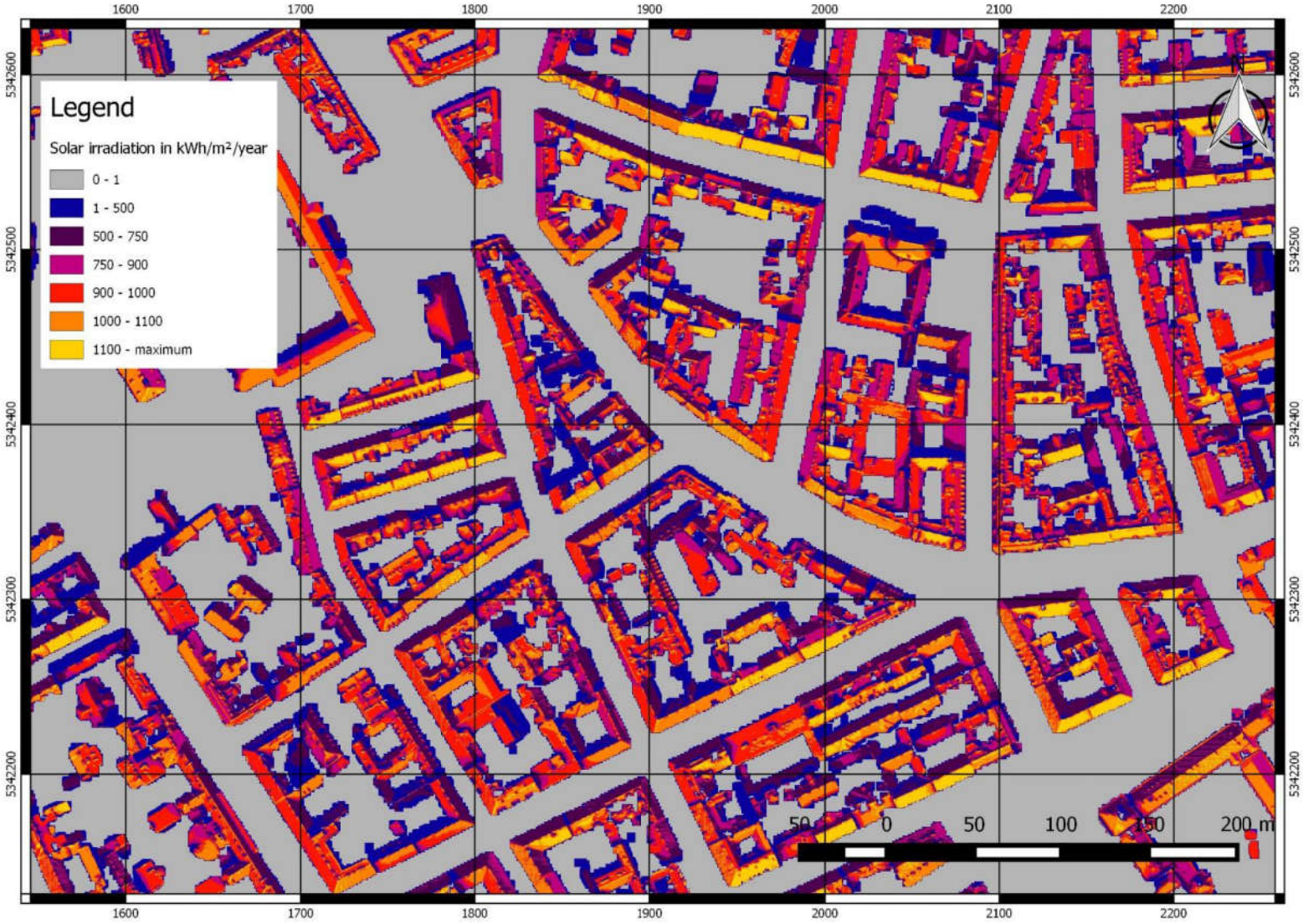
Solar irradiation map of 2015, vegetation excluded